ACCSCIENCE PUBLISHING
An International Journal of Optimization and Control: Theories & Applications
ISSN: 2146-0957 eISSN: 2146-5703
Vol.16, No.5, pp.1859-1882 (2026)
https://doi.org/10.36922/IJOCTA026060023
IJOCTA
RESEARCH ARTICLE

Control of tumor cell populations using hyperbolic functions: Stabilization and optimal therapy design

Sahar Ebrahimi Arefi[1], Mohammad Hadi Noori Skandari[1*] and Dumitru Baleanu[2]

[1]Faculty of Mathematical Sciences, Shahrood University of Technology, Shahrood, Iran
[2]Department of Computer Science and Mathematics, Lebanese American University, Beirut, Lebanon
sahar.ebrahimi70030 3@gmail.com; Math.Noori@yahoo.com; Dumitru.Baleanu@lau.edu.lb

ARTICLE INFO

Article history:
Received: February 7, 2026
Revised: June 14, 2026
Accepted: June 16, 2026
Published Online: August 20, 2026

Keywords:
Tumor cells model
Space of hyperbolic functions
Stabilizer hyperbolic control
Parameters of hyperbolic system
Optimal control of tumor cells population
Optimality conditions
Legendre-Gauss-Lobatto collocation points

AMS Classification 2010:
93C10; 49J15; 34H05; 92B05

ABSTRACT

Controlling the number of tumor cells remains a fundamental challenge in oncology due to the complex, nonlinear dynamics of tumor-immune interactions, extreme parameter scaling, and clinical constraints such as drug toxicity and the unidirectional nature of therapeutic interventions. To address these difficulties, this paper introduces a novel methodology for tumor growth control by leveraging the space of hyperbolic functions (HFs). We investigate a nonlinear model describing the dynamic interaction between effector cells and tumor cells. First, we design a stabilizing feedback control within the HFs framework, formulated as a hyperbolic tangent state feedback law. A Lyapunov-based analysis rigorously proves that this controller ensures global asymptotic stability of the desired equilibrium, where the tumor cell population is eradicated. Numerical simulations demonstrate that the proposed stabilizer drives divergent tumor growth to zero with a rapid convergence rate across various initial conditions. Furthermore, we formulate and solve an optimal control problem to simultaneously minimize the tumor cell population and the dose of a chemotherapeutic agent. The resulting optimality system, derived from Pontryagin's Minimum Principle, is efficiently discretized and solved using a numerical scheme based on hyperbolic function approximations and Legendre-Gauss-Lobatto collocation points. Simulation results confirm the efficacy of this approach, illustrating a trade-off between tumor eradication and drug usage that can be tuned via the objective function's weighting parameters. The findings collectively establish the space of hyperbolic functions as a powerful and efficient tool for both stabilization and optimal control in complex, nonlinear oncological models, offering a promising framework for designing therapeutic strategies.

1. Introduction

A tumor develops when cancer cells grow uncontrollably due to immune system failure or malfunctioning cell growth mechanisms (see[1–3]). The immune system, comprising effector cells such as NK cells and CTLs, serves as the first line of defense against tumor cells.[4] However, many cancer therapies yield only temporary outcomes, and treatment success requires eliminating enough cancer cells for the immune system to eradicate the remainder. Because immune capacity varies among individuals, treatment outcomes are not uniform. Cancer treatments include chemotherapy, immunotherapy, radiation, monoclonal antibodies, and surgery, with selection depending on the patient's condition, tumor characteristics, and disease stage. While surgery can sometimes completely remove the cancer, invasive or metastatic cancers often limit its effectiveness. Chemotherapy kills rapidly dividing cells, targeting cancer cells but also damaging healthy cells such as those

*Corresponding Author

in hair follicles, the digestive tract, and bone marrow, leading to complications like immunosuppression, gut inflammation, and hair loss. Some anticancer drugs target specific cancer cell proteins and are typically used alongside traditional chemotherapy.[5]

Given the limitations of current treatment approaches, researchers have explored novel solutions, with optimal control strategies emerging as a significant development for the precise and efficient use of therapeutic agents to minimize harm to healthy cells.[6–9] Various optimal control methods applied to tumor growth models include a delayed differential model for chemotherapy and chemo-immunotherapy,[10] a state-dependent Riccati equation scheme for chemotherapy scheduling,[11] a reinforcement learning approach for drug dosage under input constraints,[12] a linear-time-variant approximation strategy for nonlinear systems,[13] hybrid PDE-cellular automata models,[14] bang-bang optimal control,[15] and extended cancer models incorporating both immunotherapy and chemotherapy.[16,17] Khalili and Vatankhah proposed a comprehensive cancer dynamics model demonstrating that tumor cells can be eliminated with lower drug doses,[18] while multiple model predictive control (MMPC) has been applied to combination immunotherapy and chemotherapy enforcing drug toxicity and autoimmunity constraints.[19] Torres *et al.* demonstrated the effectiveness of integrating immunotherapy and chemotherapy through a multi-objective optimization framework,[20] and Burden, Fister, and colleagues investigated tumor-immune dynamics with IL-2, proving the existence of a unique optimal control characterized via adjoint systems.[21,22] Recent advances have also been made in modeling radiation therapy for cancer.[23–25] For further investigation, we refer the reader to[26–37] and contemporary oncology modeling studies.[38–44]

Recent years have witnessed significant advances in oncological research spanning medical imaging, fractional-order mathematical modeling, and molecular biology. In medical image analysis, Mahdavi proposed a U-Net model for MRI brain tumor segmentation, demonstrating encoder-decoder capabilities to automatically distinguish healthy from tumorous tissue,[45] while Khaniki *et al.* introduced a Vision Transformer with Feature Calibration and Selective Cross-Attention, achieving 99.24% accuracy for brain tumor classification.[46] In fractional-order modeling, Avazzadeh *et al.* developed an optimal approximation method for a fractional-order brain tumor model using generalized Laguerre polynomials (GLPs) with operational matrices and Lagrange multipliers,[47] and Hassani *et al.* formulated a fractional tumor-immune interaction model for lung cancer (FTIIM-LC), validating their results against real-world data.[48] At the molecular level, Bandegi *et al.* revealed that MicroRNA-873 suppresses KRAS/MAPK signaling, reduces colorectal cancer viability and invasion, and sensitizes tumor spheroids to 5-fluorouracil in a 3D microwell model, offering a potential strategy to overcome KRAS-driven chemoresistance.[49] Collectively, these recent contributions highlight the growing synergy between advanced machine learning techniques, fractional calculus, and experimental oncology in addressing complex cancer-related challenges.

Recent advances in machine-learning-assisted optimal therapy have opened new avenues for personalized cancer treatment. A quantitative systems pharmacology model combined with surrogate learning has been developed for adaptive immunotherapy dosing, where either Model Predictive Control (MPC) or Reinforcement Learning (RL) generates dynamic, personalized dosing schedules that balance tumor reduction and toxicity constraints, reducing computational burden by over 30% and improving tumor-reduction objectives by 15-25% compared to baseline rule-based dosing.[50] Furthermore, a physics-guided deep reinforcement learning framework has been proposed for personalized cancer therapy, integrating mechanistic PDE models capturing tumor-immune-drug interactions with model-free DRL agents that learn effective control policies without prior knowledge of the underlying system's structure, with Proximal Policy Optimization (PPO) achieving superior performance by balancing aggressive tumor eradication with minimal toxicity.[51] In the realm of deep-learning-enhanced biomedical control, a high-throughput spheroid-based assay facilitated by automatic spheroid segmentation using deep learning has been developed for functional precision oncology, where convolutional neural networks and transformer-based models enable automatic spheroid segmentation to measure treatment response to chemotherapy, PARP inhibitors, and radiotherapy, with the ability to discriminate between sensitive and resistant tumors based on predicting the percentage of responding spheroids.[52]

In this work, we examine a mathematical model that captures the effect of the immune system on a population of cancer cells. Employing this model

provides a clear analytical perspective and facilitates results that we anticipate will be of particular utility. First, we introduce the space of hyperbolic functions, which offers a versatile framework applicable to control systems, including tumor models. Utilizing this space, we then design and apply a stabilizing controller to the system. It is important to note that the fundamental challenges inherent in this model prevent conventional controllers from achieving practical stabilization. Specifically, these challenges can be summarized as follows: (1) the indirect influence of the control input on one of the state variables; (2) extreme parameter scaling across multiple orders of magnitude; (3) rational nonlinearities that complicate the system dynamics; and (4) a unidirectional (non-negativity) constraint on the control variable. The combination of these issues severely undermines the performance of standard control approaches.

Furthermore, we formulate an optimal control problem for the studied model, aimed at simultaneously minimizing both the population of cancer cells and the administered drug dosage. We derive the corresponding optimality conditions and, once again leveraging hyperbolic models along with transformed shifted Legendre-Gauss-Lobatto (LGL) collocation points, we discretize the resulting system. This approach yields a relatively accurate numerical approximation to the solution, enabling us to identify a therapeutic strategy that concurrently minimizes drug usage and tumor burden. Herein, we apply a hyperbolic-based control formulation to achieve this objective, modeling the chemotherapeutic agent as the control input tasked with reducing disease progression.

The main contributions of this work are threefold. First, we propose a novel stabilizing feedback control framework based on the space of hyperbolic functions (HFs), which directly addresses the fundamental challenges of the original tumor-immune model, including indirect control influence, extreme parameter scaling spanning seventeen orders of magnitude, rational non-linearities, and the unidirectional constraint $u \geq 0$. Unlike conventional methods such as the Lyapunov-stable neural network (LSNN)[53] and self-tuning fuzzy PID (STF-PID)[54] controllers, which fail to stabilize the system under the considered initial conditions, the proposed hyperbolic tangent feedback law guarantees global asymptotic stability of the desired equilibrium through a rigorous Lyapunov-based analysis. Second, we formulate and solve an optimal control problem that simultaneously minimizes tumor cell burden and chemotherapeutic drug dosage, wherein the resulting optimality system is efficiently discretized using hyperbolic function approximations combined with shifted LGL collocation points. This approach not only provides accurate numerical solutions but also overcomes the numerical ill-conditioning caused by severe parameter scaling. Third, through comparative numerical simulations, we demonstrate that the proposed hyperbolic-based method significantly outperforms both the LSNN and STF-PID approaches in terms of stabilization capability. Collectively, these contributions establish the space of HFs as a powerful and versatile mathematical framework for both stabilization and optimal control in complex oncological models.

The remainder of this article is organized as follows. Section 2 presents the mathematical model of tumor growth and introduces a control input via a suitable change of variables. In Section 3, the space of hyperbolic functions (HFs) is introduced, and a stabilizing hyperbolic tangent feedback control law is designed and applied to the model; the identification of parameters within the hyperbolic system is also addressed. Section 4 formulates an optimal control problem for the tumor cell population model. Section 5 states the optimality conditions for the aforementioned optimal control problem. In Section 6, the solution to this problem is approximated using the hyperbolic function framework. Section 7 presents numerical simulations that illustrate the effectiveness of the proposed approach. Finally, Section 8 concludes the paper.

2. Model formulation and representation

Suppose that $E(t)$ is the total population of effector cells, cytotoxic lymphocytes, and natural killer cells, and $T(t)$ represents the tumor cell population. Consider the following extended model[1]

$$\begin{cases} \dfrac{dE}{dt} &= s + \dfrac{p_1 ET}{g_1 + T} - mET - dE \\ \dfrac{dT}{dt} &= r_2 T(1 - bT) - nET \end{cases} \tag{1}$$

with initial conditions $E(0) = E_0$ and $T(0) = T_0$. Here, the quantity s represents the production rate of effector cells, and $\dfrac{p_1 ET}{g_1 + T}$ describes the Michaelis-Menten kinetics between E and T with influence coefficient p_1 (see Appendix 5.2 of[1] and **Figure 1**). The term mET accounts for the elimination of effector cells due to the killing of tumor cells. The parameter d denotes the natural death

rate of effector cells, and dE represents the corresponding decrease in their population. In the Michaels-Menten expression $\frac{p_1ET}{g_1+T}$, the quantity p_1 is the limiting value as $t \to \infty$. In the second equation of system (1), the term $r_2T(1-bT)$ describes the logistic growth of tumor cells, as determined experimentally in,[3] and nET is the number of tumor cells killed by effector cells. **Figure 1** is a simplified schematic intended to visualize the elementary flows, while the full complexity of the interactions is embedded in the system of differential equations.

Using the data obtained from different sources[1] and,[3] the parameters of system (1) were approximated and are shown in **Table 1**.

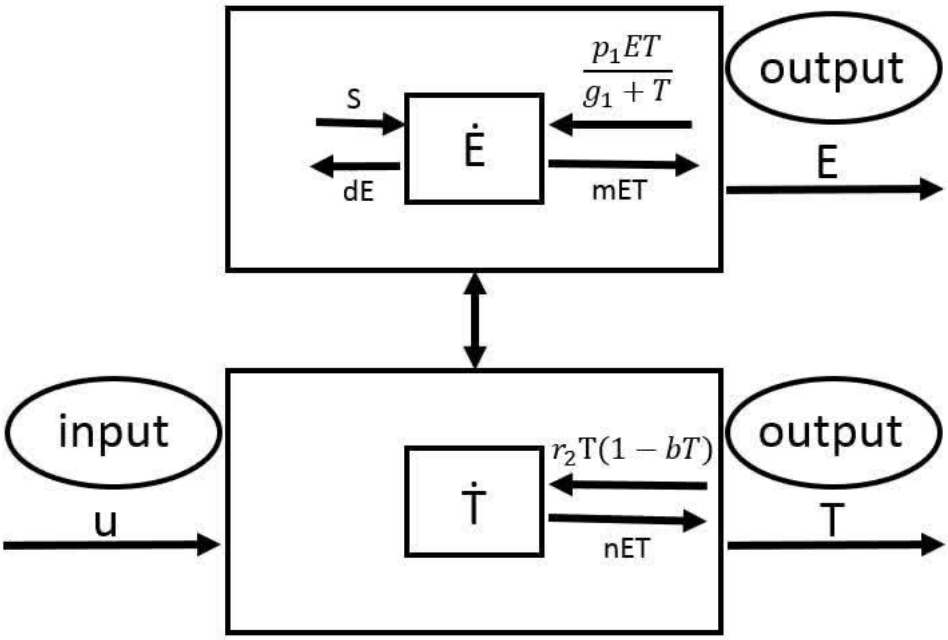

Figure 1. A simplified conceptual diagram of the key dynamic flows in the baseline model (1)

Table 1. Values of model parameters

$s = 1.3 \times 10^4 \quad \frac{cells}{dey}$	$p_1 = 0.1245 \quad day^{-1}$	$g_1 = 2.019 \times 10^7 \quad cells$
$m = 3.422 \times 10^{-10} \quad \frac{1}{dey \cdot cells}$	$d = 0.0412 \quad day^{-1}$	
$r_2 = 0.18 \quad day^{-1}$	$b = 2.0 \times 10^{-9} \quad cells^{-1}$	$n = 1.101 \times 10^{-7} \quad \frac{1}{day \cdot cells}$

Now, by the variable change $y_1 = E(t) - \frac{s}{d}$ and $y_2 = T$, the equilibrium point of system (1) is first shifted from $(E,T) = (\frac{s}{d}, 0)$ to origin $(y_1, y_2) = (0,0)$. This shift is crucial for two reasons. First, stability analysis at the origin is mathematically simpler and allows direct application of Lyapunov methods without tracking a nonzero equilibrium. Second, the hyperbolic approximation would otherwise include constant terms that complicate parameter identification and violate the structure required for the Lyapunov condition. The same transformation is standard in nonlinear control theory when the goal is regulation to a desired steady state.

After changing variables and adding the control $u \geq 0$ to the second equation, as an effective drug for reducing the number of tumor cells, we obtain the system

$$\begin{cases} \frac{dy_1}{dt} = p_1(y_1 + \frac{s}{d})\frac{y_2}{g_1+y_2} \\ -m(y_1 + \frac{s}{d})y_2 - dy_1, \\ \frac{dy_2}{dt} = r_2y_2(1-by_2) - n(y_1+\frac{s}{d})y_2 - u. \end{cases} \tag{2}$$

Note that as $y_1 \to 0$ and $y_2 \to 0$, the variable E approaches $\frac{s}{d}$, while $T \to 0$. In the following section, we first revisit the function space associated with hyperbolic tangent functions. Based on this framework, we then propose a feedback control strategy utilizing hyperbolic tangent functions to stabilize the system described above.

It is important to note that the fundamental challenges inherent in system (2) prevent conventional controllers from achieving practical stabilization. Specifically, these challenges comprise: (1) the indirect influence of the control on y_1; (2) extreme parameter scaling across seventeen orders of magnitude (ranging from 10^{-10} to 10^7), which causes severe numerical ill-conditioning in most control algorithms; (3) a rational nonlinearity of the form $\frac{y_2}{g_1+y_2}$, where $g_1 = 2.019 \times 10^7$, a term that eludes exact polynomial or affine representation; and (4) a unidirectional constraint $u \geq 0$. The combination of these issues severely undermines the performance of standard control approaches.

3. Designing stabilizer control using hyperbolic functions space

Here, we first introduce the HFs space, which is described in the work.[55] It can be proved that this space is dense in the space of continuous functions, possessing a universal approximator property.

3.1. Space of hyperbolic functions

For each $x = (x_1, \cdots, x_n) \in \Omega \subset \mathbb{R}^n$, consider the generalized variables as:

$$\begin{aligned} \bar{x}_{\theta_l+\kappa_l} &= x_l - \lambda_{\theta_l+\kappa_l}, \\ \kappa_l &= 1, 2, \cdots, \omega_l, \;\; l = 1, 2, , \cdots, n. \end{aligned} \tag{3}$$

where $\theta_l = \sum_{j=0}^{l-1} \omega_j$, $\omega_0 = 0$, $m = \sum_{l=1}^{n} \omega_l$ and λ_j for $j = 1, 2, \cdots, m$ are assumed constants. The HFs space is defined as:

$$\begin{aligned} H(\Omega) = \Bigg\{ \eta_m(x, a, b, k) = \sum_{l=1}^{m} \frac{a_l e^{k_l \bar{x}_l} + b_l e^{-k_l \bar{x}_l}}{e^{k_l \bar{x}_l} + e^{-k_l \bar{x}_l}} \\ : a_l, b_l, k_l \in \mathbb{R}, x \in \Lambda, m \geq n \Bigg\}, \end{aligned} \tag{4}$$

that the components of vector $\bar{x}$ are defined by (3). Define $z_l = \frac{a_l + b_l}{2}$ and $r_l = \frac{a_l - b_l}{2}$ for $l = 1, 2, \cdots, m$. With these, the space of HFs comes in the following form

$$\begin{aligned} H(\Omega) = \{ \eta_m(x, z, r, k) = z + r \cdot \tanh(k\bar{x}) \\ : z, r, k \in \mathbb{R}^m, x \in \Lambda, m \geq n \}, \end{aligned} \tag{5}$$

that $z = \sum_{l=1}^{m} z_l$, $r = (r_1, \cdots, r_m)$, $k = (k_1, \cdots, k_m)$, $\bar{x} = (\bar{x}_1, \cdots, \bar{x}_m)$ and

$$\begin{aligned} \tanh(k\bar{x}) = \big(\tanh(k_1\bar{x}_1), \tanh(k_2\bar{x}_2), \cdots, \\ \tanh(k_m\bar{x}_m) \big)^T. \end{aligned} \tag{6}$$

In the following theorem, we will see that if $\Omega \in \mathbb{R}^n$ is a compact set, then $H(\Omega)$ will be dense in the real continuous functions space.

Theorem 3.1. (see[55]) Assume that $\sigma(.)$ is a real continuous function on the compact set $\Omega \in \mathbb{R}^n$ and $\epsilon > 0$ is an arbitrary constant. There is an $\eta_m(., z, r, k) \in H(\Omega)$ so that $\sup_{x \in \Omega} |\sigma(x) - \eta_m(x, z, r, k)| < \epsilon$.

If we consider $m = n$, $b_l = -a_l$ and $\lambda_j = 0$ for $j, l = 1, 2, \cdots, m$, then from (4), $H(\Omega)$ is converted into

$$\begin{aligned} H(\Omega) = \Bigg\{ \eta_n(x, r, k) = \sum_{l=1}^{n} r_l \left(\frac{e^{k_l x_l} - e^{-k_l x_l}}{e^{-k_l x_l} + e^{-k_l x_l}} \right) \\ : r_l, k_l \in \mathbb{R}, \;\; l = 1, \cdots, n \Bigg\}. \end{aligned} \tag{7}$$

In addition, the space (5) can be rewritten equivalently as

$$\begin{aligned} \bar{H}(\Omega) = \{ \eta_n(x, r, k) = r \cdot \tanh(kx) : \\ r, k \in \mathbb{R}^n, \; x \in \Lambda \}, \end{aligned} \tag{8}$$

where $r = (r_1, \cdots, r_n)$ and $k = (k_1, \cdots, k_n)$.

3.2. Stabilizer hyperbolic control

Using the space of HFs, system (2) can be approximated in the neighborhood of the equilibrium point (i.e., origin) as

$$\begin{cases} \dot{y}_1 &= r_{11} \tanh(k_1 y_1) + r_{12} \tanh(k_2 y_2), \\ \dot{y}_2 &= r_{21} \tanh(k_1 y_1) + r_{22} \tanh(k_2 y_2) - u. \end{cases} \tag{9}$$

The parameters r_{ij}, $i, j = 1, 2$ can be approximated by optimization techniques (for example, the least squares method). By applying a bounded feedback control as

$$u = \gamma_1 \tanh(k_1 y_1) + \gamma_2 \tanh(k_2 y_2), \tag{10}$$

the system (9) can be rewritten as follows:

$$\dot{y} = R \tanh(ky), \tag{11}$$

where

$$y = \begin{bmatrix} y_1 \\ y_2 \end{bmatrix}, k = \begin{bmatrix} k_1 \\ k_2 \end{bmatrix}, R = \begin{bmatrix} r_{11} & r_{12} \\ r_{21} + \gamma_1 & r_{22} + \gamma_2 \end{bmatrix},$$

$$\tanh(ky) = \begin{bmatrix} \tanh(k_1 y_1) \\ \tanh(k_2 y_2) \end{bmatrix}.$$

Lemma 3.2. *For each given initial condition, $(y_1(0), y_2(0)) = (y_{10}, y_{20})$, the system (11) has a unique solution.*

Proof. We first assume that $R = \begin{bmatrix} a_{11} & a_{12} \\ a_{21} & a_{22} \end{bmatrix}$. By this, system (11) takes the following form:

$$\begin{cases} \dot{y}_1 = \psi_1(y_1, y_2) = a_{11} \tanh(k_1 y_1) \\ + a_{12} \tanh(k_2 y_2), \\ \dot{y}_2 = \psi_2(y_1, y_2) = a_{21} \tanh(k_1 y_1) \\ + a_{22} \tanh(k_2 y_2). \end{cases} \tag{12}$$

It is sufficient to show that the functions on the right-hand side of system (12) are Lipschitz continuous.[56,57] Since the right-hand side of system (12) is a linear combination of hyperbolic tangent functions, it is both continuous and differentiable. Moreover, we have:

$$\left|\frac{\partial \psi_i}{\partial y_j}\right| = |a_{ij}(1-\tanh(k_j y_j))| \leq 2|a_{ij}|, \quad i,j=1,2,$$

because $|\tanh(k_j y_j)| \leqslant 1$. Thus ψ_i for $i=1,2$ has bounded partial derivatives. Since a function with bounded first partial derivatives is globally Lipschitz continuous, we can conclude that ψ_1 and ψ_2 are Lipschitz. Specifically, a Lipschitz constant L for the vector function $\boldsymbol{\psi} = (\psi_1, \psi_2)^T$ is given by $L = 2\max_{i,j}|a_{ij}|$. Consequently, the right-hand side of system (11) [and equivalently (12)] satisfies a Lipschitz condition. By the Picard-Lindelöf theorem, this guarantees that system (11) has a unique solution for any given initial condition $(y_1(0), y_2(0)) = (y_{10}, y_{20})$. □

Theorem 3.3. *Consider the system (11) with $k > 0$. Suppose that there is a matrix $Z = \begin{bmatrix} \bar{\alpha}^2 & 0 \\ 0 & \bar{\beta}^2 \end{bmatrix}$ where $\bar{\alpha}$ and $\bar{\beta}$ are non-zero real numbers, such that*

$$ZR + R^T Z = -I, \tag{13}$$

where I is the 2×2 identity matrix. Then the system (11) is globally asymptotically stable at the origin.

Proof. Define a Lyapunov function as $V(y) = \frac{\bar{\alpha}^2}{k_1}\ln(\cosh(k_1 y_1)) + \frac{\bar{\beta}^2}{k_2}\ln(\cosh(k_2 y_2))$ where $y = (y_1, y_2)^t$. It is easy to show that $V(0) = 0$, $V(y) > 0$ for $y \neq 0$. Furthermore, if $\| y \| \to \infty$ then $V(y) \to \infty$. Now, it is sufficient to show that $\dot{V}(y) < 0$ for $y \neq 0$. By (13), we have:

$$\begin{bmatrix} \bar{\alpha}^2 & 0 \\ 0 & \bar{\beta}^2 \end{bmatrix}\begin{bmatrix} r_{11} & r_{21}+\gamma_1 \\ r_{21}+\gamma_1 & r_{22}+\gamma_2 \end{bmatrix} + \begin{bmatrix} r_{11} & r_{21}+\gamma_1 \\ r_{12} & r_{22}+\gamma_2 \end{bmatrix}\begin{bmatrix} \bar{\alpha}^2 & 0 \\ 0 & \bar{\beta}^2 \end{bmatrix} = \begin{bmatrix} -1 & 0 \\ 0 & -1 \end{bmatrix}.$$

Hence,

$$\begin{bmatrix} \bar{\alpha}^2 r_{11} & \bar{\alpha}^2 r_{12} \\ \bar{\beta}^2(r_{21}+\gamma_1) & \bar{\beta}^2(r_{22}+\gamma_2) \end{bmatrix} + \begin{bmatrix} r_{11}\bar{\alpha}^2 & (r_{21}+\gamma_1)\bar{\beta}^2 \\ r_{12}\bar{\alpha}^2 & (r_{22}+\gamma_2)\bar{\beta}^2 \end{bmatrix} = \begin{bmatrix} -1 & 0 \\ 0 & -1 \end{bmatrix}.$$

After simplification, we achieve

$$\begin{bmatrix} 1+2r_{11}\bar{\alpha}^2 & (r_{21}+\gamma_1)\bar{\beta}^2 + r_{12}\bar{\alpha}^2 \\ \bar{\beta}^2(r_{21}+\gamma_1) + r_{12}\bar{\alpha}^2 & 1+2\bar{\beta}^2(r_{22}+\gamma_2) \end{bmatrix} = \begin{bmatrix} 0 & 0 \\ 0 & 0 \end{bmatrix}.$$

Thus,

$$\bar{\alpha}^2 r_{11} = -\frac{1}{2}, \quad \bar{\alpha}^2 r_{12} + \bar{\beta}^2(r_{21}+\gamma_1) = 0, \quad \bar{\beta}^2(r_{22}+\gamma_2) = -\frac{1}{2}. \tag{14}$$

Moreover, according to the chain derivative rule, we obtain

$$\begin{aligned}\dot{V}(y) &= \frac{\bar{\alpha}^2}{k_1}\dot{y_1}\frac{k_1\sinh(k_1y_1)}{\cosh(k_1y_1)} + \frac{\bar{\beta}^2}{k_2}\dot{y_2}\frac{k_2\sinh(k_2y_2)}{\cosh(k_2y_2)} \\ &= \bar{\alpha}^2\dot{y_1}\tanh(k_1y_1) + \bar{\beta}^2\dot{y_2}\tanh(k_2y_2).\end{aligned}$$

Then, by inserting relation (9) in the above relation, we get

$$\begin{aligned}\dot{V}(y) = \alpha^2 &(r_{11}\tanh(k_1y_1) + r_{12}\tanh(k_2y_2)) \\ &\tanh(k_1y_1) + \bar{\beta}^2(r_{21}\tanh(k_1y_1) \\ &+r_{22}\tanh(k_2y_2) + u)\tanh(k_2y_2).\end{aligned}$$

and by inserting relation (10) in the above relation, we obtain

$$\begin{aligned}\dot{V}(y) =& \bar{\alpha}^2(r_{11}(k_1y_1) + r_{12} \\ &\tanh(k_2y_2))\tanh(k_1y_1) + \bar{\beta}^2(r_{21}\tanh(k_1y_1) \\ &+ r_{22}\tanh(k_2y_2) + \gamma_1\tanh(k_1y_1) \\ &+ \gamma_2\tanh(k_2y_2))\tanh(k_2y_2) \\ &= \bar{\alpha}^2 r_{11}\tanh^2(k_1y_1) + \bar{\alpha}^2 r_{12} \\ &\tanh(k_2y_2)\tanh(k_1y_1) \\ &+ \bar{\beta}^2 r_{21}\tanh(k_1y_1)\tanh(k_2y_2) \\ &+ \bar{\beta}^2 r_{22}\tanh^2(k_2y_2) + \bar{\beta}^2\gamma_1\tanh(k_1y_1) \\ &\tanh(k_2y_2) + \bar{\beta}^2\gamma_2\tanh^2(k_2y_2) \\ &= \bar{\alpha}^2 r_{11}\tanh^2(k_1y_1) + \\ &(\bar{\alpha}^2 r_{12} + \bar{\beta}^2 r_{21} + \bar{\beta}^2\gamma_1) \\ &\tanh(k_2y_2)\tanh(k_1y_1) + (\bar{\beta}^2 r_{22} \\ &+ \bar{\beta}^2\gamma_2)\tanh^2(k_2y_2) \\ &= \bar{\alpha}^2 r_{11}\tanh^2(k_1y_1) + \\ &(\bar{\alpha}^2 r_{12} + \bar{\beta}^2(r_{21}+\gamma_1)) \\ &\tanh(k_2y_2)\tanh(k_1y_1) + \bar{\beta}^2(r_{22}+\gamma_2) \\ &\tanh^2(k_2y_2).\end{aligned}$$

Therefore by (14),

$$\dot{V}(y) = -\frac{1}{2}\tanh^2(k_1y_1) - \frac{1}{2}\tanh^2(k_2y_2) < 0,$$

for any $y = (y_1, y_2) \neq (0,0)$. Thus, by Lyapunov theorem, the origin is a globally asymptotically stable point for system (11). □

By solving system (13), we can obtain $\bar{\alpha}, \bar{\beta}$, γ_1 and γ_2. In addition, control (10) can be used to stabilize system (9) globally asymptotically and to stabilize system (2) locally asymptotically.

3.3. Parameters identification of hyperbolic system

According to,[55] the parameters of the hyperbolic system (9) are obtained by solving a system of algebraic equations. For convenience, we consider system (2) in the following form:

$$\begin{cases} \dot{y}_1 = \eta_1(y_1, y_2), \\ \dot{y}_2 = \eta_2(y_1, y_2) - u. \end{cases} \tag{15}$$

The system (9) is an approximation of (15) near the equilibrium point of system (15), i.e. in a neighborhood of zero. We suggest an algebraic system to approximate the parameters r_{11}, r_{12}, r_{21}, r_{22}, k_1 and k_2. For this purpose, we assume that y_1 and y_2 are in $I = [-\sigma, \sigma]$, where $\sigma > 0$ is a given small number. We also divide I into $I_i = [-\sigma + \frac{2(i-1)\sigma}{N_1}, -\sigma + \frac{2i\sigma}{N_1}]$, $i = 1, 2, \cdots, N_1$ where N_1 is a sufficiently large number. Now, we define $y_{k,i_k} = -\sigma + \frac{2(i_k-1)\sigma}{N_1}$ for $k = 1, 2$ and $i_k = 1, 2, ..., N_1$, and solve the following system

$$\begin{cases} r_{11}\tanh(k_1 y_{1,i_1}) + r_{12}\tanh(k_2 y_{2,i_2}) \\ -\eta_1(y_{1,i_1}, y_{2,i_2}) = 0, i_1, i_2 = 1, 2, \cdots, N_1, \\ r_{21}\tanh(k_1 y_{1,i_1}) + r_{22}\tanh(k_2 y_{2,i_2}) \\ -\eta_2(y_{1,i_1}, y_{2,i_2}) = 0, i_1, i_2 = 1, 2, \cdots, N_1, \end{cases} \tag{16}$$

where r_{11}, r_{12}, r_{21}, r_{22}, k_1 and k_2 are unknown variables. Note that system (16) can be solved by optimization techniques or quasi-Newton methods, for example the Levenberg-Marquardt algorithm.[58,59]

4. Optimal control of tumor cell population

To simultaneously minimize the number of tumor cells y_2 and the dose of the administered drug u, we propose the following optimal control problem on the time interval $[0, t_f]$:

$$\text{Minimize} \quad J(y_2, u) = \int_0^{t_f} \left(\alpha y_2^2 + \beta u\right) dt \tag{17}$$

subject to the dynamical system

$$\begin{cases} \dot{y}_1 = f_1(y_1, y_2) + u, \\ \dot{y}_2 = f_2(y_1, y_2) - u, \\ y_1(0) = E_0, \quad y_2(0) = T_0, \\ 0 \le u(t) \le u_{\max}, \end{cases} \tag{18}$$

where $\alpha > 0$ and $\beta > 0$ are given weighting constants, $y(t) = (y_1(t), y_2(t))$ and

$$\begin{cases} f_1 = p_1(y_1 + \frac{s}{d})\frac{y_2}{g_1 + y_2} \\ -m\left(y_1 + \frac{s}{d}\right) y_2 - d y_1, \\ f_2 = r_2 y_2(1 - b y_2) - n\left(y_1 + \frac{s}{d}\right) y_2. \end{cases} \tag{19}$$

The control u represents the chemotherapeutic drug dosage, with the upper bound $u_{\max}$ reflecting clinical toxicity constraints. Note that the control u appears positively in the first equation (representing immune cell stimulation by the drug) and negatively in the second equation (representing tumor cell killing). This formulation captures the dual effect of chemotherapy: boosting the immune response while directly attacking tumor cells. To facilitate the theoretical analysis, we define appropriate function spaces for the state and control variables.

Definition 4.1. *The admissible state space is defined as*

$$\begin{aligned} \mathcal{D}_{state} = \{y = (y_1, y_2) \in Sob^1([0, t_f]) \\ \times Sob^1([0, t_f]) \ : \ 0 \le y_1(t) \le B_1, \\ 0 \le y_2(t) \le B_2, \ \forall t \in [0, t_f]\}, \end{aligned} \tag{20}$$

where $Sob^1([0, t_f])$ denotes the Sobolev space of functions whose first derivatives are square-integrable on $[0, t_f]$. The constants $B_1, B_2 > 0$ are physically motivated upper bounds for the effector and tumor cell populations, respectively.

Definition 4.2. *The admissible control space is defined as*

$$\begin{aligned} \mathcal{D}_{control} = \{u \in L^1([0, t_f]) \cap L^2([0, t_f]) \\ : \ 0 \le u(t) \le u_{\max}, \ \forall t \in [0, t_f]\}. \end{aligned} \tag{21}$$

4.1. Existence of an optimal control

We first establish the existence of an optimal control for the problem (17)-(18).

Theorem 4.3 (Existence of an Optimal Control)**.** *For the optimal control problem defined by* (17)-(18)*, there exists at least one optimal control $u^* \in \mathcal{D}_{control}$ and corresponding optimal state trajectory $(y_1^*, y_2^*) \in \mathcal{D}_{state}$.*

Proof. The proof follows from the Filippov-Cesari existence theorem (see,[6061]). We verify the required hypotheses:

(1) Compactness and convexity of the control set: The control set $U = [0, u_{\max}]$ is clearly compact and convex as a closed interval in $\mathbb{R}$.

(2) Carathéodory conditions: The functions $F_1(y_1, y_2, u) = f_1(y_1, y_2) + u$ and $F_2(y_1, y_2, u) = f_2(y_1, y_2) - u$ are continuous in (y_1, y_2, u) and time-independent (hence measurable in t). For any bounded set of states, the dynamics are uniformly bounded.

(3) Existence of admissible trajectories: For any admissible control $u \in \mathcal{D}_{\text{control}}$, the right-hand side functions F_1 and F_2 in (18) have bounded partial derivatives on $\mathcal{D}_{\text{state}}$. Thus, they are Lipschitz in the states, and by the

Picard-Lindelöf Theorem, a unique, absolutely continuous solution $(y_1(t), y_2(t))$ exists on $[0, t_f]$ for any given initial condition $y_1(0) = E_0$ and $y_2(0) = T_0$.

(4) Convexity of the velocity set: The velocity set is

$$\mathcal{V}(t,y) = \left\{ \begin{pmatrix} f_1(y_1,y_2) + u \\ f_2(y_1,y_2) - u \end{pmatrix} : u \in [0, u_{\max}] \right\},$$

where f_1 and f_2 are defined by (19). Since u appears linearly in both components (with coefficients $+1$ and -1), $\mathcal{V}(t,y)$ is an affine image of the convex interval $[0, u_{\max}]$, hence convex.

(5) Lower semicontinuity and coercivity: The cost integrand $L(y_2, u) = \alpha y_2^2 + \beta u$ is convex in u (hence weakly lower semicontinuous) and bounded below by 0 since $\alpha, \beta > 0$ and $y_2^2 \geq 0$, $u \geq 0$. Finally, coercivity follows from the fact that $\alpha, \beta > 0$ implies $J(y,u) \geq \beta \|u\|_{L^1}$, so $\|u\|_{L^1} \to \infty$ forces $J \to \infty$.

Having verified all hypotheses of the Filippov-Cesari Theorem, we conclude that an optimal control u^* exists for the problem (17)-(18). □

4.2. Uniqueness of the optimal control

We now establish the uniqueness of the optimal control for problem (17)-(18).

Theorem 4.4 (Uniqueness of the Optimal Solution)**.** *The optimal control problem defined by* (17)-(18) *admits at most one optimal solution* (y_1^*, y_2^*, u^*).

Proof. The proof relies on the strict convexity of the cost functional and the affine structure of the dynamics. Consider the cost functional. The integrand $L(y_2, u) = \alpha y_2^2 + \beta u$ satisfies: (i) the term αy_2^2 is strictly convex in y_2 because $\alpha > 0$, (ii) the term βu is convex in u because $\beta > 0$, (iii) the sum of a strictly convex function and a convex function is strictly convex in the pair (y_2, u). Hence, $J(y_2, u)$ is strictly convex on the admissible set. Moreover, the dynamical system can be written as

$$\dot{y} = f(y) + \tilde{f}(y)u, \tag{22}$$

where

$$f(y) = \begin{pmatrix} f_1(y_1,y_2) \\ f_2(y_1,y_2) \end{pmatrix}, \qquad \tilde{f}(y) = \begin{pmatrix} 1 \\ -1 \end{pmatrix}.$$

Thus, the dynamics are affine with respect to the control variable u. Further, the admissible control set $\mathcal{D}_{\text{control}}$ is convex. To prove the uniqueness of the optimal control, assume, for contradiction, that there exist two distinct optimal pairs $(\tilde{y}, \tilde{u})$ and $(\bar{y}, \bar{u})$ with $\tilde{u} \neq \bar{u}$ and the same optimal cost J^*. Since J is strictly convex, for any $\theta \in (0,1)$ we have

$$J(\theta\tilde{y} + (1-\theta)\bar{y},\ \theta\tilde{u} + (1-\theta)\bar{u}) < \theta J(\tilde{y}, \tilde{u}) + (1-\theta)J(\bar{y}, \bar{u}) = J^*.$$

The convex combination $\hat{u} = \theta\tilde{u} + (1-\theta)\bar{u}$ is admissible because $\mathcal{D}_{\text{control}}$ is convex. By the affine dynamics, the corresponding state trajectory is $\hat{y} = \theta\tilde{y} + (1-\theta)\bar{y}$, which is feasible, i.e., $\hat{y} \in \mathcal{D}_{\text{state}}$, it satisfies the initial condition $y_1(0) = E_0$ and $y_2(0) = T_0$, and system (22). This yields a cost lower than J^*, contradicting the optimality of J^*. Therefore, the optimal control must be unique. □

Remark 4.1. *The strict convexity of the cost functional is guaranteed by $\alpha > 0$ and $\beta > 0$. If $\alpha = 0$, the cost would depend only linearly on u, and uniqueness could fail. Similarly, $\beta > 0$ ensures the control appears with positive weight, regularizing the problem.*

5. Optimality conditions for suggested OC problem

To solve the suggested optimal control problem, we establish the necessary optimality conditions based on Pontryagin's Minimum Principle (PMP).[62] We can define the Hamiltonian function for the optimal control problem (17)-(18) as

$$H(y_1, y_2, \lambda_1, \lambda_2, u) = \alpha y_2^2 + \beta u + \lambda_1(f_1(y_1,y_2) + u) + \lambda_2 \left(f_2(y_1,y_2) - u\right),$$

where f_1 and f_2 are defined by (19), and the functions λ_1 and λ_2 are the costate variables that must be determined appropriately. The Hamiltonian function can be rewritten as

$$H(y, \lambda, u) = \underbrace{\alpha y_2^2 + \lambda_1 f_1(y_1,y_2) + \lambda_2 f_2(y_1,y_2)}_{H_0(y,\lambda)} + \underbrace{\left(\beta + \lambda_1 - \lambda_2\right)}_{W(\lambda)} u.$$

According to the PMP and the necessary optimality conditions, the optimal state variables (y_1^*, y_2^*) and the optimal control u^* must satisfy the following system together with a pair $(\lambda_1^*, \lambda_2^*)$ of costate variables:

$$\begin{cases} \dot{y}_1 = \dfrac{p_1\left(y_1 + \dfrac{s}{d}\right) y_2}{g_1 + y_2} - m\left(y_1 + \dfrac{s}{d}\right) y_2 \\ -dy_1 + u, \\ \dot{y}_2 = r_2 y_2 \left(1 - b y_2\right) - n\left(y_1 + \dfrac{s}{d}\right) y_2 - u, \\ \dot{\lambda}_1 = -\dfrac{\partial H}{\partial y_1} = -\Bigg[\left(\dfrac{p_1 y_2}{g_1 + y_2} - m y_2 - d \right) \lambda_1 \\ -n y_2 \lambda_2 \Bigg], \end{cases} \tag{23}$$

$$\begin{cases} \dot{\lambda}_2 = -\dfrac{\partial H}{\partial y_2} = -\Big[2\alpha y_2 + \lambda_1 \\ (\dfrac{p_1(y_1+\frac{s}{d})(g_1+y_2) - p_1\left(y_1+\frac{s}{d}\right)y_2}{(g_1+y_2)^2} \\ -m(y_1+\dfrac{s}{d})) + \lambda_2(r_2(1-2by_2) \\ -n\left(y_1+\dfrac{s}{d}\right))\Big], \\ u^* = \arg\min\limits_{0\leqslant u\leqslant u_{\max}} H(y_1,y_2,\lambda_1,\lambda_2,u), \\ y_1(0)=E_0,\ y_2(0)=T_0,\ \lambda_1(t_f)=0, \\ \lambda_2(t_f)=0. \end{cases}$$

Since the Hamiltonian function H is linear with respect to the control variable u and moreover $\dfrac{\partial H}{\partial u} = W(\lambda) = \beta + \lambda_1 - \lambda_2$, according to the fifth equation of system (23), the optimal control variable must satisfy

$$u^*(t) = \begin{cases} 0, & \beta+\lambda_1-\lambda_2 > 0, \\ \varphi(t), & \beta+\lambda_1-\lambda_2 = 0, \\ u_{\max}, & \beta+\lambda_1-\lambda_2 < 0. \end{cases} \tag{24}$$

where the function $0 \leqslant \varphi(t) \leqslant u_{\max}$ must be determined appropriately. Hence, according to the definition of the sign (or briefly sgn) function, we can formulate the optimal control variable u as follows

$$\begin{aligned} u^*(t) = &\left(1-\operatorname{sgn}^2(\beta+\lambda_1-\lambda_2)\right)\varphi(t) \\ &+\frac{\operatorname{sgn}^2(\beta+\lambda_1-\lambda_2)}{2} \\ &(1-\operatorname{sgn}(\beta+\lambda_1-\lambda_2))\,u_{max}. \end{aligned} \tag{25}$$

It can be shown that for any positive number Q,

$$|\operatorname{sgn}(x) - \tanh(Qx)| \leq 2e^{-2Q|x|}, \quad x \in \mathbb{R}.$$

Moreover,

$$|\operatorname{sgn}(x) - \tanh(Qx)| \leq 2e^{-2Q\chi}, \quad |x| \geq \chi.$$

Therefore, $\lim_{Q\to\infty} |\operatorname{sgn}(x) - \tanh(Qx)| = 0$ for all $x \in \mathbb{R}$, and by ((25)), $u^*(t)$ can be approximated by the following function:

$$\begin{aligned} &\Theta_Q(\varphi,\lambda_1,\lambda_2) = (1-\tanh^2(Q(\beta+\lambda_1-\lambda_2))) \\ &\varphi + \frac{\tanh^2(Q(\beta+\lambda_1-\lambda_2))}{2} \\ &\left(1-\tanh(Q(\beta+\lambda_1-\lambda_2))\right)u_{\max}, \end{aligned} \tag{26}$$

with Q representing a sufficiently large predetermined value. Since $0 \leqslant \varphi(t) \leqslant u_{\max}$, we introduce two auxiliary variables $s_1(t)$ and $s_2(t)$ to enforce this constraint via the following equivalent conditions:

$$\begin{cases} \varphi(t) - s_1^2(t) = 0, \\ u_{\max} - \varphi(t) - s_2^2(t) = 0. \end{cases} \tag{27}$$

By (26) and (27), system (23) can be written as the following algebraic-differential system

$$\begin{cases} \dot{y_1} = f_1(y_1,y_2,\lambda_1,\lambda_2,\varphi), \\ \dot{y_2} = f_2(y_1,y_2,\lambda_1,\lambda_2,\varphi), \\ \dot{\lambda_1} = g_1(y_2,\lambda_1,\lambda_2), \\ \dot{\lambda_2} = g_2(y_1,y_2,\lambda_1,\lambda_2), \\ h_1(\varphi,s_1) = 0, \\ h_2(\varphi,s_2) = 0, \\ y_1(0)=E_0, y_2(0)=T_0, \lambda_1(t_f)=0, \\ \lambda_2(t_f)=0, \end{cases} \tag{28}$$

where

$$\begin{cases} f_1(y_1,y_2,\lambda_1,\lambda_2,\varphi) = \dfrac{p_1\left(y_1+\frac{s}{d}\right)y_2}{g_1+y_2} \\ -m\left(y_1+\dfrac{s}{d}\right)y_2 - dy_1 + \Theta_Q(\varphi,\lambda_1,\lambda_2), \\ f_2(y_1,y_2,\lambda_1,\lambda_2,\varphi) = r_2y_2(1-by_2) \\ -n\left(y_1+\dfrac{s}{d}\right)y_2 - \Theta_Q(\varphi,\lambda_1,\lambda_2), \\ g_1(y_2,\lambda_1,\lambda_2) = -(\left(\dfrac{p_1y_2}{g_1+y_2} - my_2 - d\right) \\ \lambda_1 - ny_2\lambda_2), g_2(y_1,y_2,\lambda_1,\lambda_2) = -(2\alpha y_2 \\ +\lambda_1[\dfrac{p_1\left(y_1+\frac{s}{d}\right)(g_1+y_2) - \left(p_1\left(y_1+\frac{s}{d}\right)y_2\right)}{(g_1+y_2)^2} \\ -m\left(y_1+\dfrac{s}{d}\right)]) \\ -\lambda_2\left(r_2(1-2by_2) - n\left(y_1+\dfrac{s}{d}\right)\right), \\ h_1(\varphi,s_1) = \varphi(t) - s_1^2(t), \\ h_2(\varphi,s_2) = u_{max} - \varphi(t) - s_2^2(t). \end{cases}$$

Integrating both sides of the first four equations in (28) yields the following equivalent algebraic-integral system:

$$\begin{cases} y_1(t) = E_0 + \int_0^t f_1\big(y_1(\tau),y_2(\tau),\lambda_1(\tau), \\ \lambda_2(\tau),\varphi(\tau)\big)d\tau,\ \ 0 \leqslant t \leqslant t_f, \\ y_2(t) = T_0 + \int_0^t f_2\big(y_1(\tau),y_2(\tau),\lambda_1(\tau), \\ \lambda_2(\tau),\varphi(\tau)\big)d\tau,\ \ 0 \leqslant t \leqslant t_f, \\ \lambda_1(t) = -\int_t^{t_f} g_1(y_2(\tau),\lambda_1(\tau),\lambda_2(\tau))d\tau, \\ 0 \leqslant t \leqslant t_f, \\ \lambda_2(t) = -\int_t^{t_f} g_2(y_1(\tau),y_2(\tau),\lambda_1(\tau), \\ \lambda_2(\tau))d\tau, 0 \leqslant t \leqslant t_f, \\ h_1(\varphi(t),s_1(t)) = 0,\ \ 0 \leqslant t \leqslant t_f, \\ h_2(\varphi(t),s_2(t)) = 0,\ \ 0 \leqslant t \leqslant t_f. \end{cases} \tag{29}$$

Further, we define the transformations $\tau = \psi(t,s) = \dfrac{t}{t_f}s$ (for the first and second integrals in (29) and $\tau = \eta(t,s) = \dfrac{t_f-t}{t_f}s + t$ (for the third

and fourth integrals in (29)), where $0 \leqslant s \leqslant t_f$, and rewrite (29) in the following equivalent form:

$$\begin{cases} y_1(t) = E_0 + \dfrac{t}{t_f}\int_0^{t_f} f_1(y_1(\psi(t,s)), \\ y_2(\psi(t,s)), \lambda_1(\psi(t,s)), \lambda_2(\psi(t,s)), \\ \varphi(\psi(t,s)))ds, \;\; 0 \leqslant t \leqslant t_f, \\ y_2(t) = T_0 + \dfrac{t}{t_f}\int_0^{t_f} f_2(y_1(\psi(t,s)), \\ y_2(\psi(t,s)), \lambda_1(\psi(t,s)), \lambda_2(\psi(t,s)), \\ \varphi(\psi(t,s)))ds, \;\; 0 \leqslant t \leqslant t_f, \\ \lambda_1(t) = -\dfrac{t_f - t}{t_f}\int_0^{t_f} g_1(y_2(\eta(t,s)), \\ \lambda_1(\eta(t,s)), \lambda_2(\eta(t,s)))ds, \;\; 0 \leqslant t \leqslant t_f, \\ \lambda_2(t) = -\dfrac{t_f - t}{t_f}\int_0^{t_f} g_2(y_1(\eta(t,s)), \\ y_2(\eta(t,s)), \lambda_1(\eta(t,s)), \lambda_2(\eta(t,s)))ds, \\ 0 \leqslant t \leqslant t_f, \\ h_1(\varphi(t), s_1(t)) = 0, \;\; 0 \leqslant t \leqslant t_f, \\ h_2(\varphi(t), s_2(t)) = 0, \;\; 0 \leqslant t \leqslant t_f. \end{cases} \tag{30}$$

6. Approximating the solution of the OC problem by using hyperbolic functions

In the previous section, we saw that the solution of the OC problem (17)-(18) through the undertaken process led to the resolution of the algebraic-integral system (30). In this section, we suggest using the hyperbolic functions space introduced in Section 3 to approximate the solutions as follows

$$\begin{cases} y_i(t) \simeq y_i^M(t) = \bar{y}_{i,0} + \sum_{j=1}^{M} \bar{y}_{i,j} \\ \tanh\left(\bar{y}_{i,M+j}\left(t - \tau_j\right)\right), \qquad i = 1, 2, \\ \lambda_i(t) \simeq \lambda_i^M(t) = \bar{\lambda}_{i,0} + \sum_{j=1}^{M} \bar{\lambda}_{i,j} \\ \tanh\left(\bar{\lambda}_{i,M+j}\left(t - \tau_j\right)\right), \qquad i = 1, 2, \\ s_i(t) \simeq s_i^M(t) = \bar{s}_{i,0} + \sum_{j=1}^{M} \bar{s}_{i,j} \\ \tanh\left(\bar{s}_{i,M+j}\left(t - \tau_j\right)\right), \qquad i = 1, 2, \\ \varphi(t) \simeq \varphi^M(t) = \bar{\varphi}_0 + \sum_{j=1}^{M} \bar{\varphi}_j \\ \tanh\left(\bar{\varphi}_{M+j}\left(t - \tau_j\right)\right), \end{cases} \tag{31}$$

where

$$\begin{cases} \bar{\varphi}^M = (\bar{\varphi}_0, \bar{\varphi}_1, \cdots, \bar{\varphi}_{2M}), \\ \bar{y}_i^M = (\bar{y}_{i,0}, \bar{y}_{i,1}, \cdots, \bar{y}_{i,2M}), \\ \bar{\lambda}_i^M = (\bar{\lambda}_{i,0}, \bar{\lambda}_{i,1}, \cdots, \bar{\lambda}_{i,2M}), \\ \bar{s}_i^M = (\bar{s}_{i,0}, \bar{s}_{i,1}, \cdots, \bar{s}_{i,2M}), \\ \tau^M = (\tau_1, \tau_2, \cdots, \tau_M), \end{cases} \tag{32}$$

are unknown. After this approximation, we proceed to apply a well-known discretization scheme. To this end, let $\zeta_0 = -1 < \zeta_1 < \cdots < \zeta_N = 1$ denote the LGL collocation points over the interval $[-1, 1]$. These points are dense in the interval $[-1, 1]$ when N goes to infinity. Also, they are the roots of the following polynomial

$$\bar{P}_{N+1}(\zeta) = \left(1 - \zeta^2\right)\frac{dP_N(\zeta)}{d\zeta}, \tag{33}$$

where $P_N(.)$ is the Legendre polynomial of degree N, which is defined by the following recursive relation

$$\begin{aligned} &(i+1)P_{i+1}(\zeta) = (2i+1) + P_i(\zeta) - iP_{i-1}(\zeta), \\ &\quad i \geqslant 1, \end{aligned} \tag{34}$$

where $P_0(\zeta) = 1$ and $P_1(\zeta) = \zeta$ for $\zeta \in [-1, 1]$. We should transfer the LGL points $\{\zeta_k\}_{k=0}^N$ to the interval $[0, t_f]$. This can be done by the following linear transformation

$$t_k = \frac{t_f}{2}(\zeta_k + 1), \quad k = 0, 1, \cdots, N. \tag{35}$$

By applying the above shifted LGL points and the approximations in (31), the system (30) is discretized as

$$\begin{cases} Y(\bar{y}_1^M, \tau^M, t_k) = E_0 + \dfrac{t_k}{t_f}\int_0^{t_f} f_1(y_1^M(\psi(t_k,s)), \\ y_2^M(\psi(t_k,s)), \lambda_1^M(\psi(t_k,s)), \lambda_2^M(\psi(t_k,s)), \\ \varphi(\psi(t_k,s)))ds, \\ Y(\bar{y}_2^M, \tau^M, t_k) = T_0 + \dfrac{t_k}{t_f}\int_0^{t_f} f_2(y_1^M(\psi(t_k,s)), \\ y_2^M(\psi(t_k,s)), \lambda_1^M(\psi(t_k,s)), \lambda_2^M(\psi(t_k,s)), \\ \varphi(\psi(t_k,s)))ds, \\ \Lambda(\bar{\lambda}_1^M, \tau^M, t_k) = -\dfrac{t_f - t_k}{t_f}\int_0^{t_f} g_1(y_2^M(\eta(t_k,s)), \\ \lambda_1^M(\eta(t_k,s)), \lambda_2^M(\eta(t_k,s)))ds, \\ \Lambda(\bar{\lambda}_2^M, \tau^M, t_k) = -\dfrac{t_f - t_k}{t_f}\int_0^{t_f} g_2(y_1^M(\eta(t_k,s)), \\ y_2^M(\eta(t_k,s)), \lambda_1^M(\eta(t_k,s)), \lambda_2^M(\eta(t_k,s)))ds, \\ h_1\big(\Phi(\bar{\varphi}^M, \tau^M, t_k), S(\bar{s}_1^M, \tau^M, t_k)\big) = 0, \\ h_2\big(\Phi(\bar{\varphi}^M, \tau^M, t_k), S(\bar{s}_2^M, \tau^M, t_k)\big) = 0, \\ k = 0, 1, ..., N. \end{cases} \tag{36}$$

where

$$\begin{cases} Y(\bar{y}_i^M, \tau^M, t_k) = \bar{y}_{i,0} + \sum_{j=1}^{M} \bar{y}_{i,j} \\ \tanh\left(\bar{y}_{i,M+j}\left(t_k - \tau_j\right)\right), \\ \Lambda(\bar{\lambda}_i^M, \tau^M, t_k) = \bar{\lambda}_{i,0} + \sum_{j=1}^{M} \bar{\lambda}_{i,j} \\ \tanh\left(\bar{\lambda}_{i,M+j}\left(t_k - \tau_j\right)\right), \\ S(\bar{s}_i^M, \tau^M, t_k) = \bar{s}_{i,0} + \sum_{j=1}^{M} \bar{s}_{i,j} \\ \tanh\left(\bar{s}_{i,M+j}\left(t_k - \tau_j\right)\right), \\ \Phi(\bar{\varphi}^M, \tau^M, t_k) = \bar{\varphi}_0 + \sum_{j=1}^{M} \bar{\varphi}_j \\ \tanh\left(\bar{\varphi}_{M+j}\left(t_k - \tau_j\right)\right), \\ i = 1, 2, \;\; k = 0, 1, ..., N. \end{cases} \tag{37}$$

The following lemma is required to approximate the integrals in system (36).

Lemma 6.1. *Assume that $\{t_j\}_{j=1}^N$ are the shifted LGL points on the interval $[0, t_f]$. Then for any polynomial $q(.)$ of degree at most $(2N-1)$ we have*

$$\int_0^{t_f} q(t)dt = \sum_{j=1}^{N} w_j q\left(t_j\right), \tag{38}$$

where the weights $\{w_j\}_{j=1}^N$ *satisfy the following relation*

$$w_j = \frac{t_f}{(N^2+N)\left(P_N\left(2t_j-1\right)\right)^2}, j = 1, 2, \ldots, N.$$

Proof. Suppose that $q(.)$ is a given polynomial of degree at most $(2N-1)$. Define $\zeta_j = 2t_j - 1$ for $j = 1, 2, \ldots, N$ where $\{t_j\}_{j=1}^N$ are the shifted LGL points on the interval $[0, t_f]$. Also, take $\bar{q}(\zeta) = q\left(\frac{t_f}{2}(\zeta+1)\right)$ for $-1 \leq \zeta \leq 1$. From Theorem 3.29 in,[63] we have

$$\int_{-1}^{1} \bar{q}(\zeta)d\zeta = \sum_{j=1}^{N} \bar{w}_j \bar{q}\left(\zeta_j\right) \tag{39}$$

where

$$\bar{w}_j = \frac{2}{(N^2+N)\left(P_N\left(\zeta_j\right)\right)^2}, \quad j = 1, 2, \ldots, N,$$

and $P_N(.)$ is the Legendre polynomial of degree N. Hence, by the transformation $t = \frac{t_f}{2}(\zeta+1)$ and relation (39), we get

$$\int_0^{t_f} q(t)dt = \frac{t_f}{2}\int_{-1}^{1} q\left(\frac{t_f}{2}(\zeta+1)\right)$$
$$d\zeta = \frac{t_f}{2}\int_{-1}^{1}\bar{q}(\zeta)d\zeta = \frac{t_f}{2}\sum_{j=1}^{N}\bar{w}_j\bar{q}\left(\zeta_j\right)$$
$$= \sum_{j=1}^{N} w_j q\left(t_j\right)$$

where

$$w_j = \frac{t_f}{2}\bar{w}_j = \frac{t_f}{(N^2+N)\left(P_N\left(2t_j-1\right)\right)^2}, \quad j = 1, 2, \ldots, N.$$

□

Relation (38) can be used to approximate the integral of any continuous function on the interval $[0, t_f]$, including those appearing in system (36). Accordingly, this system can be transformed into the following algebraic form:

$$\begin{cases} Y(\bar{y}_1^M, \tau^M, t_k) = E_0 + \frac{t_k}{t_f}\sum_{l=0}^{N} w_l \\ f_1(y_1^M(\psi(t_k, s_l)), y_2^M(\psi(t_k, s_l))), \\ \lambda_1^M(\psi(t_k, s_l)), \\ \lambda_2^M(\psi(t_k, s_l)), \varphi(\psi(t_k, s_l))), \\ Y(\bar{y}_2^M, \tau^M, t_k) = T_0 + \frac{t_k}{t_f}\sum_{l=0}^{N} w_l \\ f_2(y_1^M(\psi(t_k, s_l)), y_2^M(\psi(t_k, s_l))), \\ \lambda_1^M(\psi(t_k, s_l)), \\ \lambda_2^M(\psi(t_k, s_l)), \varphi(\psi(t_k, s_l))), \\ \Lambda(\bar{\lambda}_1^M, \tau^M, t_k) = -\frac{t_f - t_k}{t_f}\sum_{l=0}^{N} w_l \\ g_1(y_2^M(\eta(t_k, s_l)), \lambda_1^M(\eta(t_k, s_l)), \\ \lambda_2^M(\eta(t_k, s_l))), \\ \Lambda(\bar{\lambda}_2^M, \tau^M, t_k) = -\frac{t_f - t_k}{t_f}\sum_{l=0}^{N} w_l \\ g_2(y_1^M(\eta(t_k, s_l)), y_2^M(\eta(t_k, s_l)), \lambda_1^M(\eta(t_k, s_l)), \\ \lambda_2^M(\eta(t_k, s_l))), \\ h_1\big(\Phi(\bar{\varphi}^M, \tau^M, t_k), S(\bar{s}_1^M, \tau^M, t_k)\big) = 0, \\ h_2\big(\Phi(\bar{\varphi}^M, \tau^M, t_k), S(\bar{s}_2^M, \tau^M, t_k)\big) = 0, \\ k = 0, 1, ..., N, \end{cases} \tag{40}$$

with the corresponding unknown variables introduced in **Equation (32)**.

7. Numerical results

The simulation results are organized and discussed across two separated subsections. Note that the values of the parameters are provided in **Table 1** and remain fixed throughout the manuscript, including this section. Moreover, $\frac{s}{d} \approx 3.155 \times 10^5$ cells.

7.1. Numerical simulation for designing stabilizing control

We now present numerical simulations to illustrate the results of the approach outlined in Subsection 3.2. Consider model (1), or equivalently, system (2). The behavior of system (2) with $u = 0$ and initial conditions $(y_1(0), y_2(0)) = (40, 100)$, $(35, 80)$, and $(30, 60)$ is shown in **Figures 2–4**, respectively. These plots demonstrate that the uncontrolled system is divergent and the tumor cell population grows significantly.

Next, using the parameter identification method described in Subsection 3.3, the corresponding hyperbolic system (9) is obtained as:

$$\begin{cases} \dot{y}_1 &= -0.0196\tanh(2.4357y_1) \\ &\quad +0.0031\tanh(0.5181y_2), \\ \dot{y}_2 &= 1.0217\times10^{-13}\tanh(2.4357y_1) \\ &\quad +0.2421\tanh(0.5181y_2) - u. \end{cases} \tag{41}$$

It is important to note that the right-hand side of the hyperbolic system (41) can effectively approximate that of the main dynamical system (2), particularly in regions near the origin. The accuracy of this approximation is quantified by the absolute errors between the two systems, which are presented in **Figure 5**. As shown in this figure, the approximation errors remain small when the state variables are sufficiently close to zero, validating the use of the hyperbolic model as a local approximation of the original dynamics. Note that our objective is not merely to perform this approximation, but rather to design an effective controller for the original nonlinear system. This can be accomplished by designing a controller for

the hyperbolic system. Indeed, we will demonstrate that the closed-loop controller developed for the hyperbolic system is capable of stabilizing the original system.

Furthermore, solving **Equation (13)** yields the values $\gamma_1 = 2.1040$, $\gamma_2 = 13.7099$, $\bar{\alpha} = 5.0503$, and $\bar{\beta} = 0.1927$. Hence, according to (10), the following hyperbolic feedback control stabilizes model (2), or equivalently system (1):

$$u = 2.1040 \tanh(2.4357 y_1) + 13.7099 \tanh(0.5181 y_2). \quad (42)$$

The behavior of the variables in system (2) under the hyperbolic stabilizing feedback (HSF) control u given by (42) is shown in **Figures 6–8** for the initial conditions $(y_1(0), y_2(0)) = (40, 100)$, $(35, 80)$, and $(30, 60)$, respectively. We observe that the trajectories converge to zero, that is, $y_1 \to 0$ and $y_2 \to 0$, with a satisfactory rate of convergence. Consequently, $E \to \dfrac{s}{d}$ and $T \to 0$. Thus, the proposed feedback control (42) effectively reduces the tumor cell population.

Note that despite the fundamental challenges of system (2), including the indirect influence of control on y_1, extreme parameter scaling spanning seventeen orders of magnitude from 10^{-10} to 10^{7} (which causes severe numerical ill-conditioning in most control algorithms), the rational nonlinearity $\dfrac{y_2}{g_1 + y_2}$ with $g_1 = 2.019 \times 10^7$ that cannot be exactly represented by polynomial or affine approximations, and the unidirectional constraint $u \geq 0$, the proposed feedback law achieves practical stabilization. The use of tanh activation functions naturally enforces the non-negativity constraint $u \geq 0$ while providing smooth, bounded control action. Numerical simulations confirm that the closed-loop system remains bounded and stable for the given initial conditions. Thus, while the system poses significant stabilization challenges, a suitably designed hyperbolic feedback law can achieve practical stability.

To provide a rigorous comparison and further substantiate the effectiveness of the proposed method in stabilizing system (2), two distinct control approaches, designated as LSNN method[53] and STF-PID control method,[54] are implemented under the initial conditions $(y_1(0), y_2(0)) = (40, 100)$. The corresponding results are presented in **Figures 9–11**. Although the output state variables show relatively similar behavior for the two different controllers, neither the LSNN method nor the STF-PID method can stabilize the system. This comparative analysis clearly demonstrates the superior performance of the stabilizing controller proposed in this work.

7.2. Numerical simulation for designing optimal control

Consider the OC problem (17)–(18). We present simulation results of the method discussed in Section 6. The accuracy of the obtained approximate solutions is evaluated using the residual error defined by system (40). The parameters are set as

$$t_f = 3, \quad E_0 = 5, \quad T_0 = 4, \quad u_{\max} = 1.$$

The following cases are examined:

Case I. The optimal solutions are simulated for $\alpha = 1$, $\beta = 3$ and different values of M and N. The results are shown in **Figures 12** and **13**, and **Table 2**.

Case II. The optimal solutions are simulated for $\alpha = 3$, $\beta = 1$ and different values of M and N. The results are shown in **Figures 14** and **15**, and **Table 3**.

Case III. The optimal solutions are simulated for $\alpha = 3$, $\beta = 3$ and different values of M and N. The results are shown in **Figures 16** and **17**, and **Table 4**.

The results confirm that, using the proposed method, the number of tumor cells $y_2(\cdot)$ and the administered drug dosage $u(\cdot)$ can be minimized simultaneously, with the trade-off governed by the weighting coefficients α and β in the objective functional.

To further demonstrate the effectiveness of the proposed method for the optimal control problem (17)–(18), the direct pseudospectral method[64] is implemented under the same initial conditions for Case I. The results are presented in **Figure 18** and **Table 5**. A direct comparison confirms that the proposed method is notably more stable and better suited for solving the optimal control problem considered herein. It is worth noting that while both methods employ LGL nodes as collocation points, they differ in their basis functions for approximating optimal solutions:[64] uses Lagrange polynomials, whereas the proposed method uses hyperbolic tangent basis functions. Therefore, for optimal control problems with complex dynamical systems such as (18), the hyperbolic tangent function space can provide better performance than Lagrange polynomials.

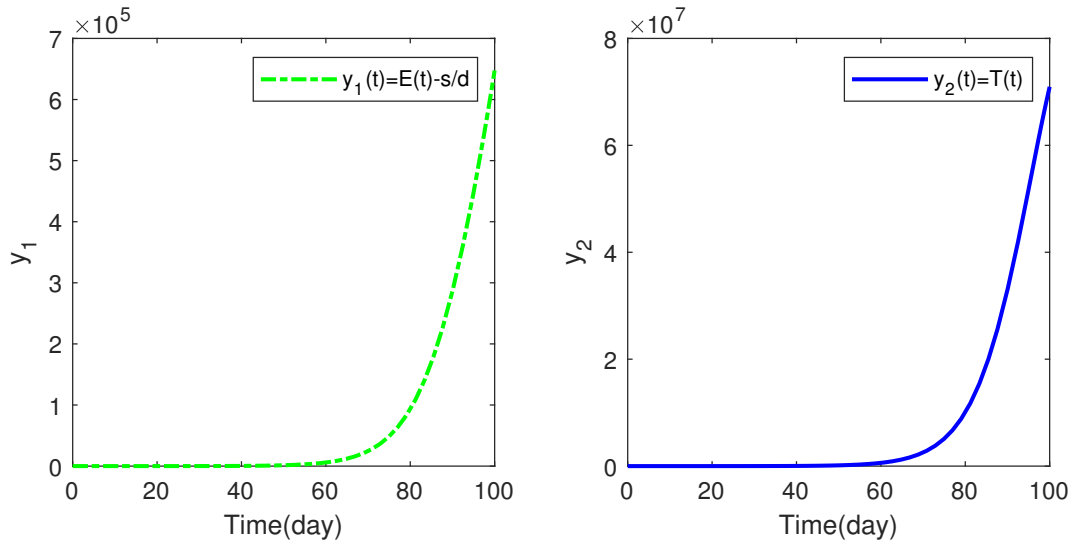

Figure 2. Behavior of system (2), without control, for initial conditions $(y_1(0), y_2(0)) = (40, 100)$

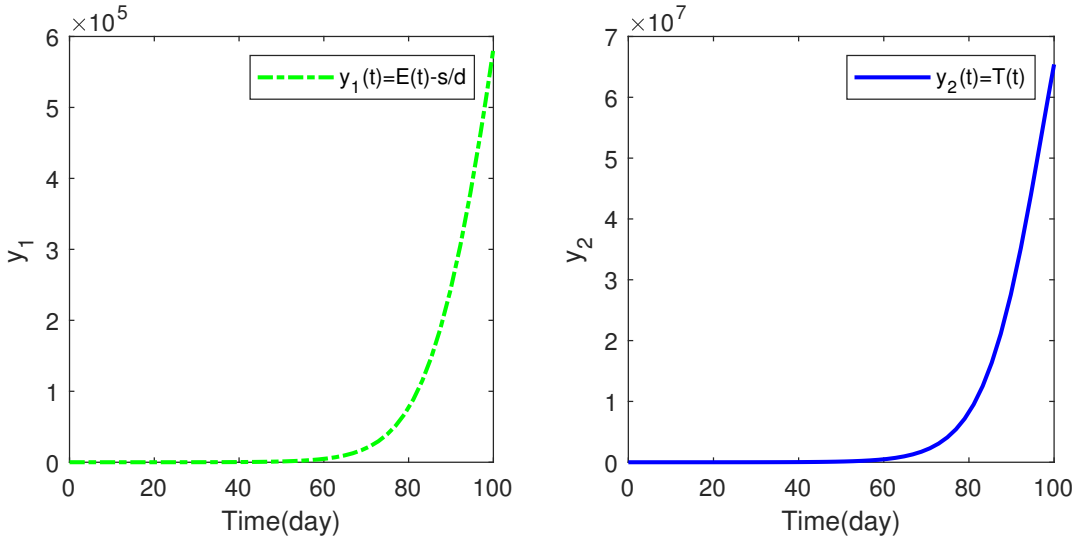

Figure 3. Behavior of system (2), without control for initial conditions $(y_1(0), y_2(0)) = (35, 80)$

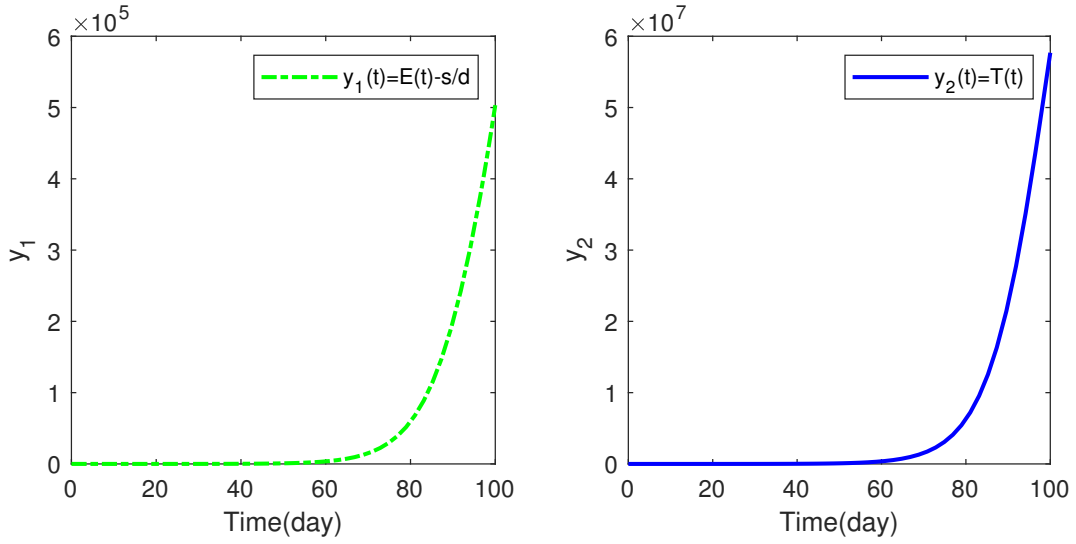

Figure 4. Behavior of system (2), without control, for initial conditions $(y_1(0), y_2(0)) = (30, 60)$

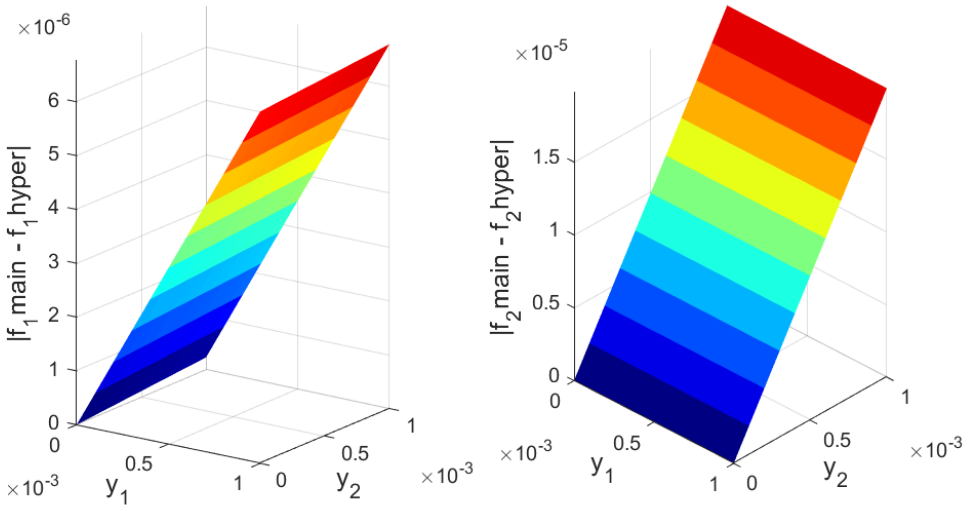

Figure 5. Absolute error in approximating the right-hand side of the main system (2) with the hyperbolic system (41)

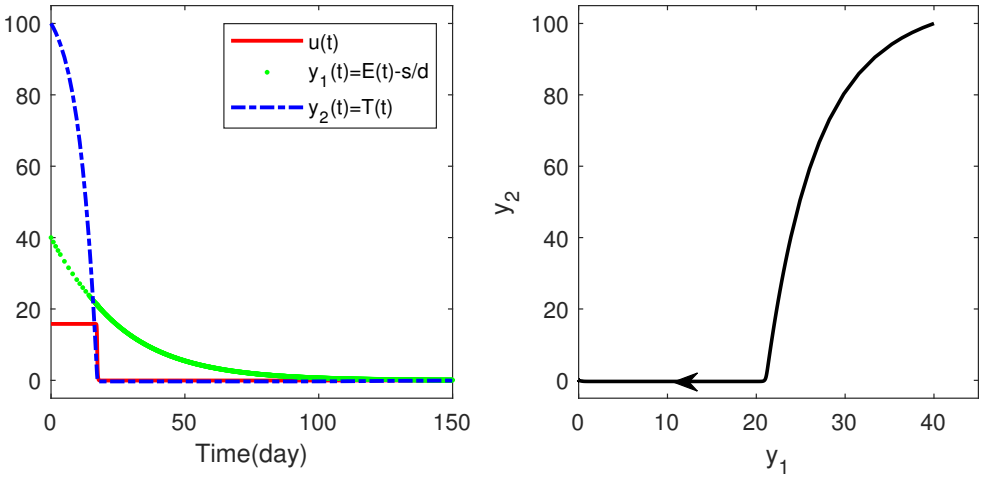

Figure 6. Behavior of system (2) under the HSF control (42) for initial conditions $(y_1(0), y_2(0)) = (40, 100)$

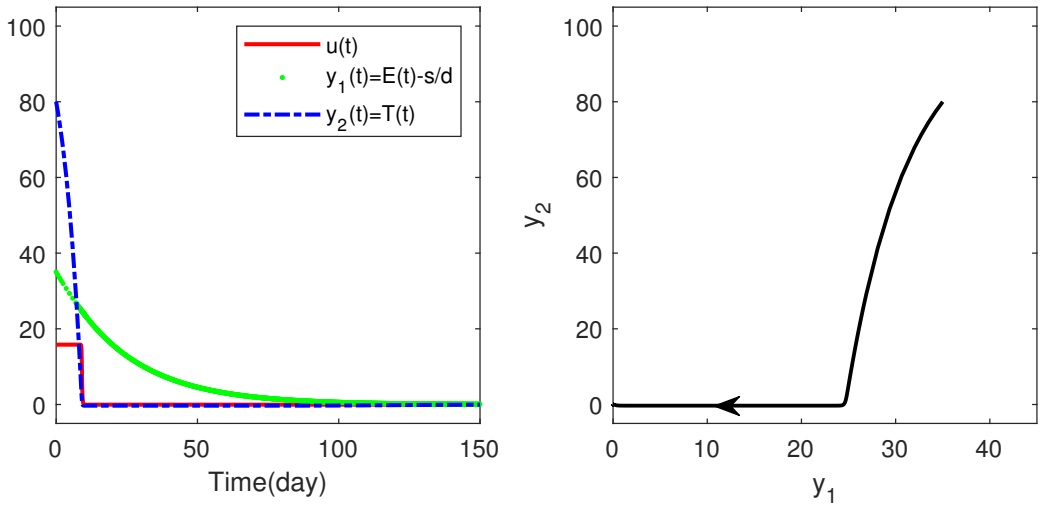

Figure 7. Behavior of system (2) under the HSF control (42) with initial conditions $(y_1(0), y_2(0)) = (35, 80)$

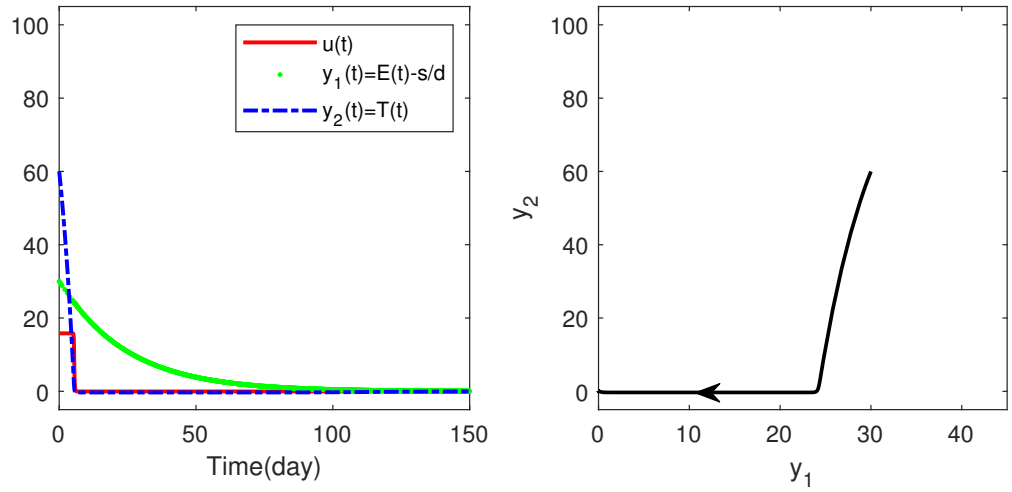

Figure 8. Behavior of system (2) under the HSF control (42) for initial conditions $(y_1(0), y_2(0)) = (30, 60)$

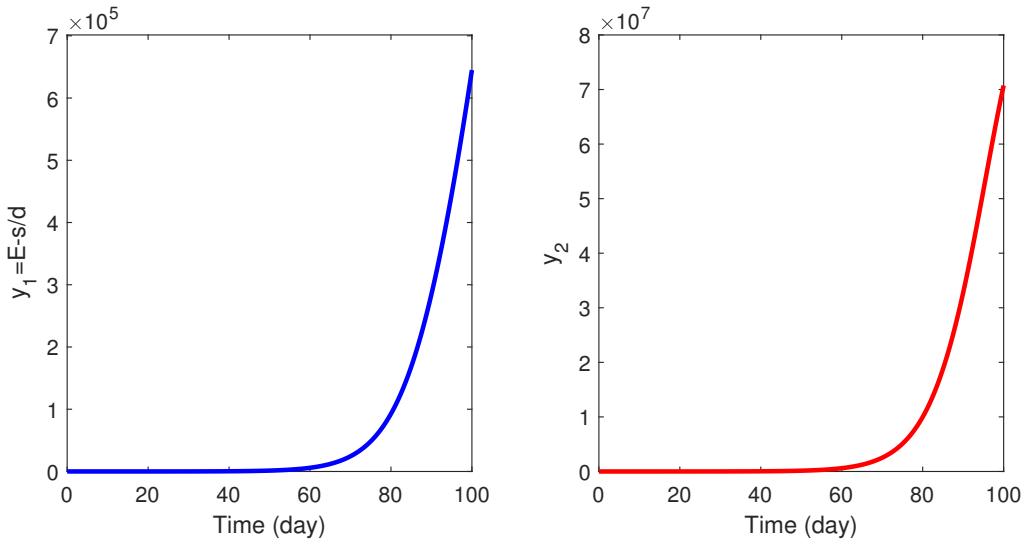

Figure 9. Behavior of system (2) under the LSNN control[53] for initial conditions $(y_1(0), y_2(0)) = (40, 100)$

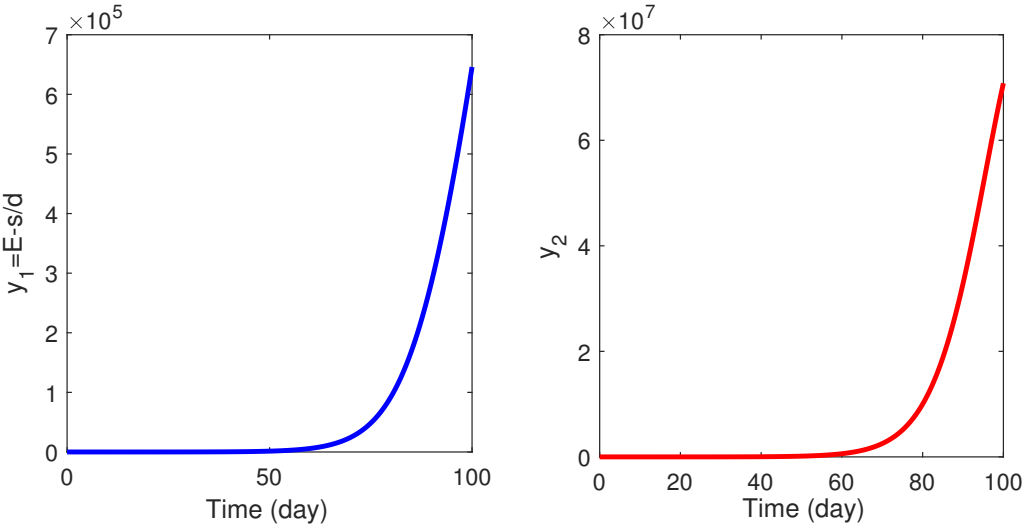

Figure 10. Behavior of system (2) under the STF-PID control[54] for initial conditions $(y_1(0), y_2(0)) = (40, 100)$

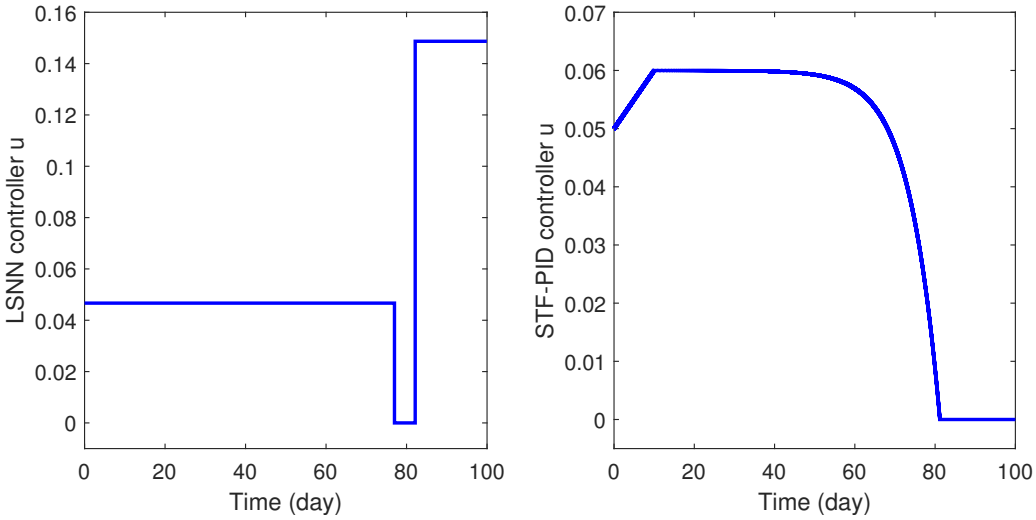

Figure 11. Comparison of the LSNN[53] and STF-PID[54] controllers for system (2) with initial conditions $(y_1(0), y_2(0)) = (40, 100)$

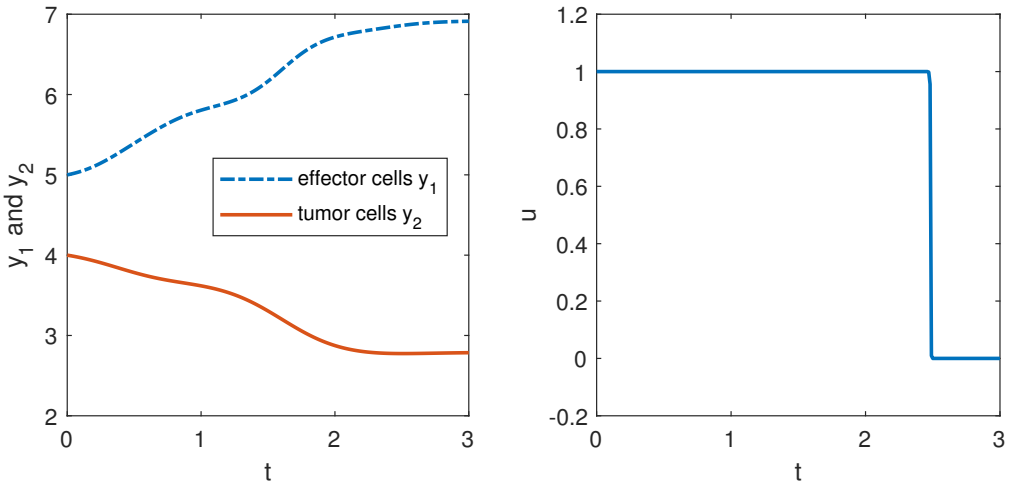

Figure 12. Obtained optimal solutions using the proposed method for Case I with $N = 4$

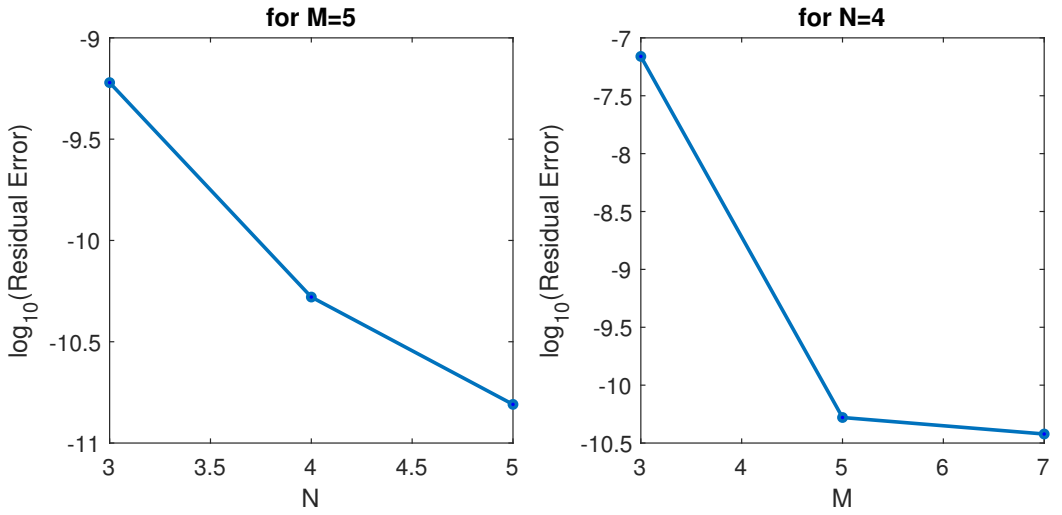

Figure 13. Logarithm of the residual error of the proposed method for Case I with different values of M and N

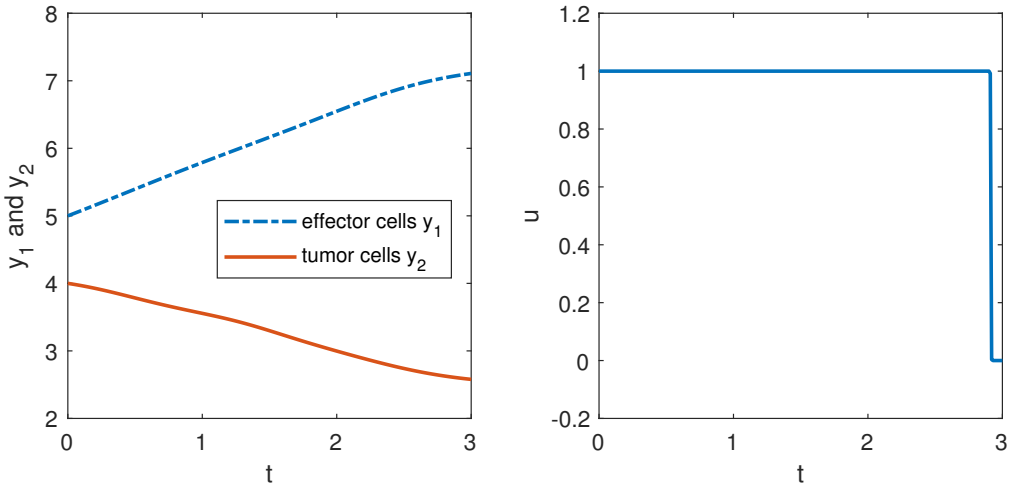

Figure 14. Obtained optimal solutions using the proposed method for Case II with $N = 4$

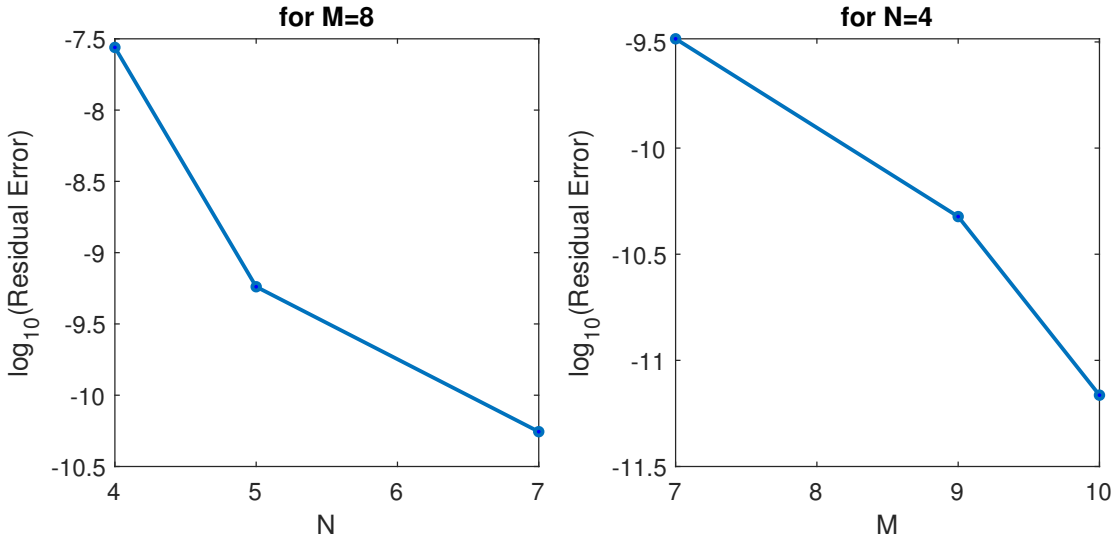

Figure 15. Logarithm of the residual error of the proposed method for Case II with different values of M and N

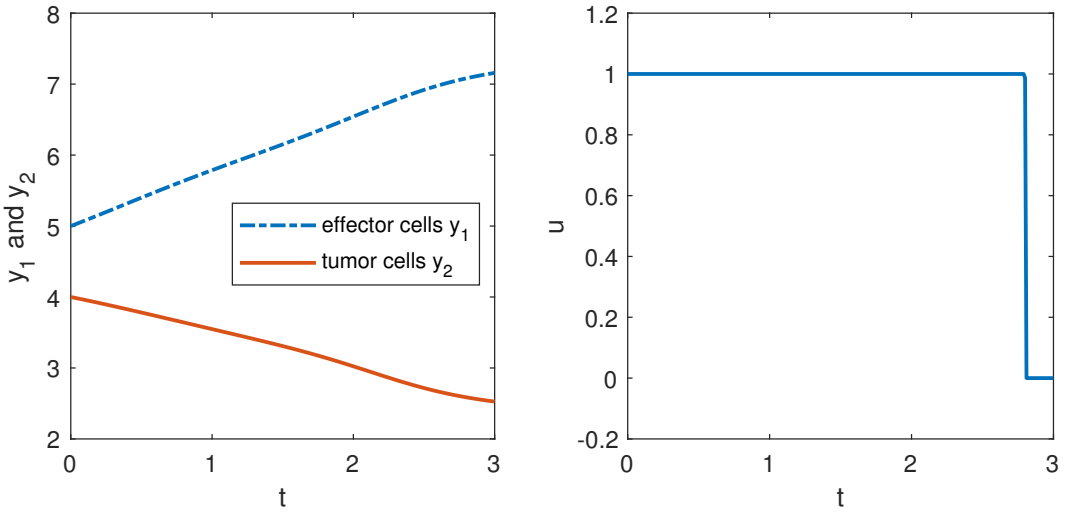

Figure 16. Obtained optimal solutions using the proposed method for Case III with $N = 5$

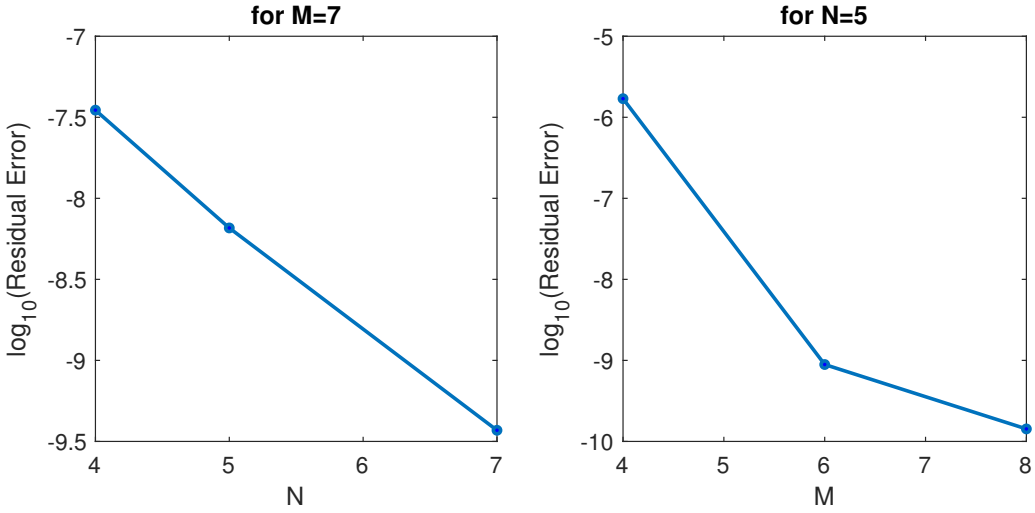

Figure 17. Logarithm of the residual error of the proposed method for Case III with different values of M and N

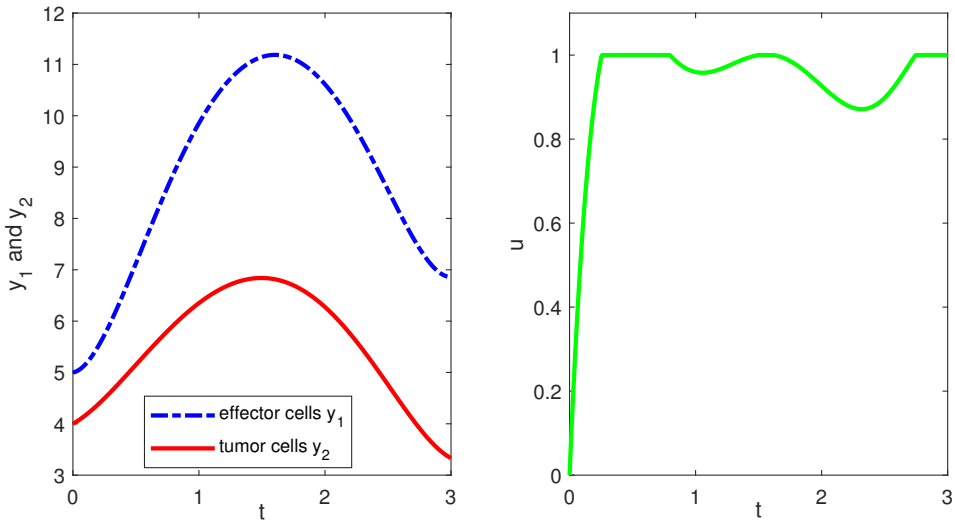

Figure 18. Obtained optimal solutions using the pseudospectral method[64] for Case I with $N = 6$

Table 2. Obtained values of the objective functional J using the proposed method for $\alpha = 1$, $\beta = 3$

M, N	$M = 5, N = 3$	$M = 5, N = 4$	$M = 5, N = 5$	$N = 4, M = 3$	$N = 4, M = 5$	$N = 4, M = 7$
J	56.77139206	56.65863426	56.74206986	56.80320637	56.65863426	56.86467288

Table 3. Obtained values of the objective functional J using the proposed method for $\alpha = 3$, $\beta = 1$

M, N	$M = 8, N = 4$	$M = 8, N = 5$	$M = 8, N = 7$	$N = 4, M = 7$	$N = 4, M = 9$	$N = 4, M = 10$
J	146.57362058	146.27584654	146.15392174	146.31189014	146.41264910	146.55374727

Table 4. Obtained values of the objective functional J using the proposed method for $\alpha = 3$, $\beta = 3$

M, N	$M = 7, N = 4$	$M = 7, N = 5$	$M = 7, N = 7$	$N = 5, M = 4$	$N = 5, M = 6$	$N = 5, M = 8$
J	152.42880080	152.27763193	152.00533478	152.46531327	152.27149524	152.26847894

Table 5. Obtained values of the objective functional J using the pseudospectral method[64] for $\alpha = 1$, $\beta = 3$

N	$N = 2$	$N = 3$	$N = 4$	$N = 5$	$M = 6$
J	42.350062	47.634485	67.375147	73.616457	103.548544

8. Conclusions and suggestions

8.1. Summary of contributions

The main contributions of this work are summarized as follows:

Hyperbolic Function Framework: We formally introduced the space of hyperbolic functions (HFs) and demonstrated its applicability as a universal approximator for nonlinear systems. This space provided the foundation for both controller design and the numerical solution of the resulting optimality conditions. It is worth emphasizing that the HF framework inherently respects the unidirectional constraint $u \geq 0$ through the boundedness of the tanh function, thereby circumventing one of the major challenges associated with conventional control methods.

Stabilizing Control Design: A hyperbolic tangent state feedback controller was systematically designed. A rigorous Lyapunov-based analysis proved that this controller guarantees global asymptotic stability of the desired equilibrium point where the tumor cell population is eradicated $(y_1, y_2) \to (0, 0)$, corresponding to $E \to s/d$ and $T \to 0$. The parameter identification method (Subsection 3.3) successfully translated the original biological model into an equivalent hyperbolic system, enabling this control design. Notably, despite the rational nonlinearity $\frac{y_2}{g_1+y_2}$ that cannot be exactly represented by polynomial or affine approximations, the HF-based approximation error remains small in the neighborhood of the origin, as quantified in **Figure 5**.

Optimal Control Strategy: We formulated an optimal control problem to minimize a composite cost functional balancing tumor cell burden and chemotherapeutic drug usage. The necessary optimality conditions, derived via PMP, resulted in a challenging two-point boundary value problem. A key innovation was the efficient discretization of this problem using hyperbolic function approximations in conjunction with shifted Legendre-Gauss-Lobatto (LGL) collocation points.

8.2. Synthesis of numerical findings

The numerical simulations robustly confirmed the theoretical developments:

Stabilization Efficacy: As shown in **Figures 2–8**, the uncontrolled system exhibits divergent tumor growth. In stark contrast, the application of the proposed hyperbolic stabilizing feedback (HSF) control (42) drives the state trajectories to zero with a rapid and consistent convergence rate across diverse initial conditions (e.g., (40, 100), (35, 80), (30, 60)). This validates the controller's practical effectiveness in suppressing tumor proliferation. More importantly, while both the LSNN and STF-PID controllers fail to stabilize the system under the same conditions (according to **Figures 9–11**), the proposed HSF control achieves practical stabilization, underscoring the necessity of tailoring the control law to the specific structural challenges of the model.

Optimal Control Performance: The results for the optimal control problem (Cases I-III in Section 7.2) illustrate the method's precision and flexibility. The algorithm successfully generated optimal drug administration profiles $u^*(t)$ that strategically balance the competing goals of tumor reduction and drug minimization, as dictated by the weighting parameters α and β. The low residual errors (e.g., **Figures 13, 15** and **17**) and the convergence of the objective functional values (**Tables 2–4**) with increasing discretization parameters M and N attest to the numerical scheme's accuracy and stability. Furthermore, compared to the direct pseudospectral method using Lagrange polynomials, the proposed hyperbolic basis functions yield notably more stable solutions for the complex dynamical system under consideration.

8.3. Broader implications

Collectively, this work establishes the space of HFs as a powerful and efficient dual-purpose tool for oncological modeling. It is effective for:

- Analytical Stabilization: Providing a Lyapunov-stable, bounded control law with proven global convergence.
- Numerical Optimization: Enabling accurate approximation schemes for solving complex optimal control problems arising from nonlinear dynamics.

The methodology offers a promising mathematical framework for in-silico design and testing of therapeutic strategies, where explicit trade-offs between treatment efficacy and toxicity can be quantitatively explored. It is also worth reiterating that the ability of the HF-based approach to

handle extreme parameter scaling, rational nonlinearities, and control constraints without numerical ill-conditioning represents a significant advancement over standard control algorithms.

8.4. Future research directions

Building on this foundation, several avenues for future research are promising:

- Model Complexity: Extend the HF-based framework to more complex and spatially heterogeneous models, such as those governed by partial differential equations (PDEs), which can account for tumor invasion and microenvironmental interactions.
- Multi-therapy Integration: Incorporate combined-modality therapies (e.g., immunotherapy, radiotherapy, anti-angiogenic drugs) as multiple control inputs within the optimal control framework to study synergistic effects.
- Clinical Parameterization: Validate and calibrate the model using longitudinal clinical data to enhance its predictive power and potential for personalized treatment planning.
- Robust and Adaptive Control: Investigate the design of robust HF-based controllers that account for system uncertainties, parameter variations, and measurement noise, moving towards adaptive therapeutic protocols.

In conclusion, this research demonstrates that HFs provide a versatile and computationally effective paradigm for both the analysis and control of nonlinear tumor dynamics, opening new pathways for the mathematical design of cancer treatment strategies. The comparative failure of LSNN and STF-PID methods further highlights that the proposed HF-based stabilization is not merely an incremental improvement but a necessary structural remedy for the specific challenges posed by the tumor-immune model.

Acknowledgments

None.

Funding

None.

Conflict of interest

The authors declare that they have no competing interests.

Author contributions

Conceptualization: Mohammad Hadi Noori Skandari and Dumitru Baleanu
Formal analysis: Mohammad Hadi Noori Skandari and Dumitru Baleanu
Investigation: Sahar Ebrahimi Arefi
Methodology: Sahar Ebrahimi Arefi and Mohammad Hadi Noori Skandari
Software: Sahar Ebrahimi Arefi and Mohammad Hadi Noori Skandari
Writing–original draft: Sahar Ebrahimi Arefi
Writing–review & editing: Mohammad Hadi Noori Skandari

Availability of data

Not applicable.

AI tools statement

During the preparation of this work, the authors used AI-assisted language tools solely for the purpose of improving the readability and language quality of the manuscript, as well as for literature review assistance. No AI tools were employed in the development of the mathematical formulations, the design of the numerical methods, the implementation of the simulations, or the interpretation of the results. All theoretical derivations, computational implementations, and data analyses were performed entirely by the authors. The authors take full responsibility for the content and accuracy of this paper.

References

1. Ferrara J. *A study of nonlinear dynamics in mathematical biology.* Master's thesis. Jacksonville, FL: University of North Florida; 2013. Accessed January 10, 2026. https://digitalcommons.unf.edu/etd/448/
2. Abbas AK, Lichtman AH, Pober JS. *Cytokines in Cellular and Molecular Immunology.* Philadelphia, PA: B Saunders Company; 1997. Accessed January 10, 2026. https://books.google.com/books/about/Cellular_and_Molecular_Immunology.html?id=zwRrAAAAMAAJ
3. Kuznetsov VA, Makalkin IA, Taylor MA, Perelson AS. Nonlinear dynamics of immunogenic tumors: parameter estimation and global bifurcation analysis. *Bull Math Biol.* 1994;56(2):295-321. https://doi.org/10.1016/S0092-8240(05)80260-5
4. Rosenberg SA, Yang JC, Topalian SL, *et al.* Treatment of 283 consecutive patients with metastatic melanoma or renal cell cancer using high-dose bolus interleukin 2. *JAMA.* 1994;271(12):907-913. Accessed January 10, 2026. https://pubmed.ncbi.nlm.nih.gov/8120958/
5. Sharma S, Samanta GP. Dynamical behaviour of a tumor-immune system with chemotherapy and optimal control. *J Nonlinear Dyn.*

2013;2013:608598.
https://doi.org/10.1155/2013/608598

6. De Pillis LG, Radunskaya A. A mathematical tumor model with immune resistance and drug therapy: an optimal control approach. *Comput Math Methods Med*. 2001;3(2):79-100.
https://doi.org/10.1080/10273660108833067
7. Matveev AS, Savkin AV. Application of optimal control theory to analysis of cancer chemotherapy regimens. *Syst Control Lett*. 2002;46(5):311-321.
https://doi.org/10.1016/s0167-6911(02)00134-2
8. Panetta JC, Fister KR. Optimal control applied to competing chemotherapeutic cell-kill strategies. *SIAM J Appl Math*. 2003;63(6):1954-1971.
https://doi.org/10.1137/S0036139902413489
9. Boltjanskij VG. *Mathematical Methods of Optimal Control*. New York, NY: Holt, Rinehart and Winston; 1971. Accessed January 10, 2026.
https://www.semanticscholar.org/paper/73d2272ab86c52ac25b31c0e39b1fe5fc71f2d35
10. Ravindran NS, Sheriff MM, Krishnapriya P. Analysis of tumour-immune evasion with chemo-immuno therapeutic treatment with quadratic optimal control. *J Biol Dyn*. 2017;11(1):480-503.
https://doi.org/10.1080/17513758.2017.1381280
11. Itik M, Salamci MU, Banks SP. SDRE optimal control of drug administration in cancer treatment. *Turk J Electr Eng Comput Sci*. 2010;18(5):715-730.
https://doi.org/10.3906/elk-1001-411
12. Chen L, Zhang YW, Zhang SC. Optimal drug dosage control strategy of immune systems using reinforcement learning. *IEEE Access*. 2023;11:1269-1279.
https://doi.org/10.1109/ACCESS.2022.3233567
13. Itik M, Salamci MU, Banks SP. Optimal control of drug therapy in cancer treatment. *Nonlinear Anal Theory Methods Appl*. 2009;71(12):e1473-e1486.
https://doi.org/10.1016/j.na.2009.01.214
14. Enderling H, Anderson AR, Chaplain MA, Munro AJ, Vaidya JS. Mathematical modelling of radiotherapy strategies for early breast cancer. *J Theor Biol*. 2006;241(1):158-171.
https://doi.org/10.1016/j.jtbi.2005.11.015
15. De Pillis LG, Radunskaya A. The dynamics of an optimally controlled tumor model: A case study. *Math Comput Modelling*. 2003;37(11):1221-1244.
https://doi.org/10.1016/s0895-7177(03)00133-x
16. De Pillis LG, Gu W, Radunskaya AE. Mixed immunotherapy and chemotherapy of tumors: modeling, applications and biological interpretations. *J Theor Biol*. 2006;238(4):841-862.
https://doi.org/10.1016/j.jtbi.2005.06.037
17. De Pillis LG, Gu W, Fister KR, *et al*. Chemotherapy for tumors: An analysis of the dynamics and a study of quadratic and linear optimal controls. *Math Biosci*. 2007;209(1):292-315.
https://doi.org/10.1016/j.mbs.2006.05.003
18. Khalili P, Vatankhah R. Optimal control design for drug delivery of immunotherapy in chemoimmunotherapy treatment. *Comput Methods Programs Biomed*. 2023;229:107248.
https://doi.org/10.1016/j.cmpb.2022.107248
19. Sharifi N, Ozgoli S, Ramezani A. Multiple model predictive control for optimal drug administration of mixed immunotherapy and chemotherapy of tumours. *Comput Methods Programs Biomed*. 2017;144:13-19.
https://doi.org/10.1016/j.cmpb.2017.03.012
20. De Paiva Torres M, Lobato FS, Libotte GB. Exploring trade-offs in drug administration for cancer treatment: A multi-criteria optimization approach. *Math Biosci*. 2025;382:109404.
https://doi.org/10.1016/j.mbs.2025.109404
21. Burden TN, Ernstberger J, Fister KR. Optimal control applied to immunotherapy. *Discrete Contin Dyn Syst Ser B*. 2004;4(1):135-146.
https://doi.org/10.3934/dcdsb.2004.4.135
22. Fister KR, Donnelly JH. Immunotherapy: an optimal control theory approach. *Math Biosci Eng*. 2005;2(3):499-510.
https://doi.org/10.3934/mbe.2005.2.499
23. Zarepisheh M, Hong L, Zhou Y, *et al*. Automated intensity modulated treatment planning: The expedited constrained hierarchical optimization (ECHO) system. *Med Phys*. 2019;46(7):2944-2954.
https://doi.org/10.1002/mp.13572
24. Thor M, Iyer A, Jiang J, *et al*. Deep learning auto-segmentation and automated treatment planning for trismus risk reduction in head and neck cancer radiotherapy. *Phys Imaging Radiat Oncol*. 2021;19:96-101.
https://doi.org/10.1016/j.phro.2021.07.009
25. Fu A, Taasti VT, Zarepisheh M. Distributed and scalable optimization for robust proton treatment planning. *Med Phys*. 2023;50(1):633-642.
https://doi.org/10.1002/mp.15897
26. Arciero JC, Jackson TL, Kirschner DE. A mathematical model of tumor-immune evasion and siRNA treatment. *Discrete Contin Dyn Syst Ser B*. 2004;4(1):39-58.
https://doi.org/10.3934/dcdsb.2004.4.39
27. Bellomo N, Preziosi L. Modelling and mathematical problems related to tumor evolution and its interaction with the immune system. *Math Comput Modelling*. 2000;32(3-4):413-452.
https://doi.org/10.1016/s0895-7177(00)00143-6
28. de Pillis LG, Radunskaya AE, Wiseman CL. A validated mathematical model of cell-mediated immune response to tumor growth. *Cancer Res*. 2005;65(17):7950-7958.
https://doi.org/10.1158/0008-5472.CAN-05-0564
29. Nani F, Freedman HI. A mathematical model of cancer treatment by immunotherapy. *Math Biosci*. 2000;163(2):159-199.
https://doi.org/10.1016/s0025-5564(99)00058-9

30. Pinho STRD, Bacelar FS, Andrade RFS, Freedman HI. A mathematical model for the effect of anti-angiogenic therapy in the treatment of cancer tumours by chemotherapy. *Nonlinear Anal Real World Appl*. 2013;14(1):815-828. https://doi.org/10.1016/j.nonrwa.2012.07.034
31. Takayanagi T, Ohuchi A. A mathematical analysis of the interactions between immunogenic tumor cells and cytotoxic T lymphocytes. *Microbiol Immunol*. 2001;45(10):709-715. https://doi.org/10.1111/j.1348-0421.2001.tb01305.x
32. Yafia R. Dynamics analysis and limit cycle in a delayed model for tumor growth with quiescence. *Nonlinear Anal Model Control*. 2006;11(1):95-110. https://doi.org/10.15388/NA.2006.11.1.14766
33. De Pillis LG, Fister KR, Gu W, *et al*. Optimal control of mixed immunotherapy and chemotherapy of tumors. *J Biol Syst*. 2008;16(01):51-80. https://doi.org/10.1142/S0218339008002435
34. Sharma S, Samanta GP. Analysis of the dynamics of a tumor-immune system with chemotherapy and immunotherapy and quadratic optimal control. *Differ Equ Dyn Syst*. 2016;24(2):149-171. https://doi.org/10.1007/s12591-015-0250-1
35. Zouhri S, Saadi S, Elmouki I, Hamdache A, Rachik M. Mixed immunotherapy and chemotherapy of tumors: optimal control approach. *Int J Comput Sci Issues*. 2013;10(4):81-97. Accessed January 10, 2026. https://www.researchgate.net/publication/282329493_Mixed_Immunotherapy_and_Chemotherapy_of_Tumors_Optimal_Control_Approach
36. Castiglione F, Piccoli B. Cancer immunotherapy, mathematical modeling and optimal control. *J Theor Biol*. 2007;247(4):723-732. https://doi.org/10.1016/j.jtbi.2007.04.003
37. Castiglione F, Piccoli B. Optimal control in a model of dendritic cell transfection cancer immunotherapy. *Bull Math Biol*. 2006;68(2):255-274. https://doi.org/10.1007/s11538-005-9014-3
38. Bukkuri A. Optimal control analysis of combined chemotherapy-immunotherapy treatment regimens in a PKPD cancer evolution model. *Biomath*. 2020;9(1):ID-2002137. https://doi.org/10.11145/j.biomath.2020.02.137
39. Naik PA, Zu J, Naik MU. Stability analysis of a fractional-order cancer model with chaotic dynamics. *Int J Biomath*. 2021;14(06):2150046. https://doi.org/10.1142/S1793524521500467
40. Zhang Z, Li S, Si P, Li X, He X. A tumor-immune model with mixed immunotherapy and chemotherapy: Qualitative analysis and optimal control. *J Biol Syst*. 2022;30(02):339-364. https://doi.org/10.1142/S0218339022500127
41. Sabir Z, Munawar M, Abdelkawy MA, *et al*. Numerical investigations of the fractional-order mathematical model underlying immune-chemotherapeutic treatment for breast cancer using the neural networks. *Fractal Fract*. 2022;6(4):184. https://doi.org/10.3390/fractalfract6040184
42. Liliopoulos SG, Stavrakakis GS, Dimas KS. Linear and non-linear optimal control methods to determine the best chemotherapy schedule for most effectively inhibiting tumor growth. *Biomedicines*. 2025;13(2):315. https://doi.org/10.3390/biomedicines13020315
43. Homayounzade M, Sajadian S. Designing a resilient controller for cancer immunotherapy: Application to a fractional-order tumour-immune model. *IET Syst Biol*. 2025;19(1):e70019. https://doi.org/10.1049/syb2.70019
44. Khan A, Abdeljawad T, Abdel-Aty M, Almutairi DK. Digital analysis of discrete fractional order cancer model by artificial intelligence. *Alex Eng J*. 2025;118:115-124. https://doi.org/10.1016/j.aej.2025.01.036
45. Mahdavi Z. MRI brain tumors detection by proposed U-Net model. In: *Proceedings of the MOL2NET'22, Conference on Molecular, Biomedical, Computational & Network Science and Engineering*. 8th ed. MDPI; 2023. https://doi.org/10.3390/mol2net-08-13726
46. Khaniki MAL, Mirzaeibonehkhater M, Manthouri M, *et al*. Vision transformer with feature calibration and selective cross-attention for brain tumor classification. *Iran J Comput Sci*. 2025;8:335-347. https://doi.org/10.1007/s42044-024-00220-w
47. Avazzadeh Z, Hassani H, Ebadi MJ, Agarwal P, Poursadeghfard M, Naraghirad E. Optimal approximation of fractional order brain tumor model using generalized Laguerre polynomials. *Iran J Sci*. 2023;47:501-513. https://doi.org/10.1007/s40995-022-01388-1
48. Hassani H, Avazzadeh Z, Agarwal P, *et al*. A study on fractional tumor-immune interaction model related to lung cancer via generalized Laguerre polynomials. *BMC Med Res Methodol*. 2023;23:189. https://doi.org/10.1186/s12874-023-02006-3
49. Bandegi M, Biltekin E, Akay YM, Ozpolat B, Akay M. MicroRNA-873 suppresses viability and invasion of colorectal cancer through KRAS/MAPK signaling and sensitizes tumor spheroids to 5-fluorouracil in a 3D microwell model. *IEEE Open J Eng Med Biol*. 2026;7:146-157. https://doi.org/10.1109/OJEMB.2026.3678868
50. Aburub F, Mohammad SI, Al Oraini B, Alenazi SA, Vasudevan A, Mohammad AI. Machine-learning guided optimal control of cancer immunotherapy: A quantitative systems pharmacology model for adaptive dosing. *Lett Biomathematics*. 2026. Accessed January 10, 2026. https://lettersinbiomath.org/manuscript/index.php/lib/article/view/528
51. Rabie F, Eslahchi MR, Tefagh M, *et al*. Physics-guided deep reinforcement learning for personalized PDE control in cancer therapy optimization.

Eng Comput. 2026;42:96.
https://doi.org/10.1007/s00366-026-02315-3

52. Haspels HN, *et al*. High-throughput spheroid-based assay for functional breast cancer precision medicine facilitated by deep learning. *Commun Med*. 2026;6:94.
https://doi.org/10.1038/s43856-025-01359-8
53. Tan WGY, Xiao M, Wu G, Wu Z. Lyapunov stable neural networks for modelling and control of nonlinear systems. *Int J Control*. 2026;99(2):578-594.
https://doi.org/10.1080/00207179.2025.2525544
54. Miskon MT, Rahiman MHF, Taib MN. Improving coffee roast yield consistency with self-tuned fuzzy-PID controller. *Int J Innov Eng*. 2025;17(2).
https://doi.org/10.30880/ijie.2025.17.02.025
55. Noori Skandari MN, Ghaznavi M, Abedian M. Stabilizer control design for nonlinear systems based on the hyperbolic modelling. *Appl Math Modelling*. 2019;67:413-429.
https://doi.org/10.1016/j.apm.2018.11.006
56. Arnold VI. *Ordinary Differential Equations*. Berlin, Germany: Springer-Verlag; 1992. Accessed January 10, 2026.
https://link.springer.com/book/9783540345633
57. Uchiyama Y, Iwasa Y, Yamaguchi S. Optimal composition of chloride cells for osmoregulation in a randomly fluctuating environment. *J Theor Biol*. 2022;537:110166.
https://doi.org/10.1016/j.jtbi.2022.111016
58. Fodor L, Jakovetić D, Krejić N, Malaspina G. Parallel inexact Levenberg-Marquardt method for nearly-separable nonlinear least squares. *J Glob Optim*. 2025;8:1-29.
https://doi.org/10.1007/s10898-025-01494-5
59. Lv X, Yu Z. A modified Levenberg-Marquardt algorithm for low order-value optimization problem. *J Appl Math Comput*. 2024;70(6):5629-5644.
https://doi.org/10.1007/s12190-024-02140-1
60. Cesari L. *Optimization Theory and Applications: Problems with Ordinary Differential Equations*. New York, NY: Springer-Verlag; 1983.
https://doi.org/10.1007/978-1-4613-8165-5
61. Fleming WH, Rishel RW. *Deterministic and Stochastic Optimal Control*. New York, NY: Springer-Verlag; 1975.
https://doi.org/10.1007/978-1-4612-6380-7
62. Pontryagin LS, Boltyanskii VG, Gamkrelidze RV, Mishchenko EF. *The Mathematical Theory of Optimal Processes*. New York, NY: Interscience Publishers; 1962.
https://doi.org/10.1201/9780203749319
63. Shen J, Tang T, Wang LL. *Spectral Methods: Algorithms, Analysis and Applications*. Vol 41. Berlin, Germany: Springer Science and Business Media; 2011.
https://doi.org/10.1007/978-3-540-71041-7
64. Qi Gong, Ross IM, Kang W, Fahroo F. Connections between the covector mapping theorem and convergence of pseudospectral methods for optimal control. *Comput Optim Appl*. 2008;41:307-335.
https://doi.org/10.1007/s10589-007-9102-4

Sahar Ebrahimi Arefi *is a doctoral candidate in the Department of Applied Mathematics at Shahrood University of Technology, Shahrood, Iran. She received her Master of Science in Applied Mathematics from Ferdowsi University of Mashhad, Mashhad, Iran, and her Bachelor of Science from Hakim Sabzevari University, Sabzevar, Iran.*
https://orcid.org/0009-0002-0211-1030.

Mohammad Hadi Noori Skandari *is an Associate Professor of Applied Mathematics in the Faculty of Mathematical Sciences at Shahrood University of Technology, Shahrood, Iran. He received his Ph.D. in Control and Optimization from Ferdowsi University of Mashhad, Iran, in 2013. His research interests include control systems, spectral and pseudospectral methods, ordinary and partial differential equations, fractional models, and optimization and optimal control problems.*
https://orcid.org/0000-0002-0900-1099.

Dumitru Baleanu *is a Professor of Mathematics in the Department of Computer Science and Mathematics at the Lebanese American University, Beirut, Lebanon. His research interests are broad and include fractional dynamics and its applications, fractional differential equations, mathematical biology, mathematical physics, soliton theory, Lie symmetries, dynamic systems on time scales, image processing, and the wavelet method. He is a pioneer in the field of fractional variational principles and their applications in control theory.*
https://orcid.org/0000-0002-0286-7244.

An International Journal of Optimization and Control: Theories & Applications (https://accscience.com/journal/ijocta)